

MONTHLY WEATHER REVIEW

JAMES E. CASKEY, JR., Editor

Volume 89, Number 12

Washington, D.C.

December 1961

ON THE RADIATIVE EQUILIBRIUM AND HEAT BALANCE OF THE ATMOSPHERE

SYUKURO MANABE

U.S. Weather Bureau, Washington, D.C.
and

FRITZ MÖLLER

Meteorological Institute, University of Munich
[Manuscript received April 20, 1961; revised September 22, 1961]

ABSTRACT

In order to incorporate the effect of radiation into the numerical experiment of the general circulation of the atmosphere, a simplified scheme for computing the radiative temperature change is constructed. The effects included are long wave radiation by water vapor, carbon dioxide, and ozone and the absorption of solar radiation by these three gases. The absorptivities of these gases are determined based upon the recent results of laboratory experiments and those of theoretical computations. The effects of clouds are not included.

By use of this scheme the radiative equilibrium temperature is computed for various latitudes and seasons as asymptotic solutions of an initial value problem. To a certain degree the radiative equilibrium solutions reveal some of the typical characteristics of stratospheric temperature and tropopause height variations.

Radiative heat budgets of the atmosphere are also computed and compared with the results of the computations of radiative equilibrium. This comparison is helpful for understanding the role of radiative processes and also suggests the kinds of effect we should expect from other thermal processes in the atmosphere.

CONTENTS

1. Introduction	503	8. Discussion of results	517
2. Temperature change due to long wave radiation	505	Radiative equilibrium	517
Water vapor	506	Heat budget	525
Carbon dioxide and ozone	506	9. Conclusions	528
Pressure and temperature effect	507	10. Critical comments and future work	529
Overlapping	507	Acknowledgments	529
3. Temperature change due to absorption of solar radiation	507	Appendix I. Vertical coordinate system	529
4. Absorptivities of long wave radiation	508	Appendix II. Emissivities and absorptivities	530
Water vapor	508	Appendix III. Finite difference equations	530
Carbon dioxide	509	References	530
Ozone	510		
5. Absorptivities of solar radiation	511		
Water vapor	511		
Carbon dioxide	512		
Ozone	513		
6. Distribution of gases	513		
Water vapor	513		
Carbon dioxide	514		
Ozone	514		
7. Computation of radiative equilibrium	514		

1. INTRODUCTION

One of the most successful attempts in the study of the general circulation of the atmosphere was the numerical experiment performed by Phillips [49]. Assuming a steady heat source and sink in low and high latitudes respectively, and numerically integrating the system of the equations of motion and the thermodynamical equation, he obtained a latitudinal distribution of temperature

with such typical characteristics of the actual atmosphere as the polar front accompanied by a strong jet stream. This study has been further extended by Smagorinsky [57]. After assuming distributions of heat source and sink corresponding to winter and summer, his calculation exhibited the typical polar front accompanied by very strong cyclone waves in winter, and rather small pole to equator temperature contrast with very weak baroclinic activities in summer. Though the contrast between summer and winter which he obtained is too large, due to the lack of oceans in his model, this experiment provides very good clues to our understanding of the mechanism of seasonal variations of temperature and wind field in the atmosphere.

However, for the sake of computational simplicity, both of these calculations are based upon a two-level model. As a natural consequence of this simplification the static stability was assumed constant with space and time. This model, therefore, is not capable of simulating the vertical temperature distribution of the atmosphere. It is a very challenging problem, however, to simulate the latitudinal distribution of the height of the tropopause, that of the temperature in the stratosphere, and the polar inversion in the lower troposphere. In order to do this it is necessary to build a model which has a high resolution (many levels) in the vertical direction and which includes the various thermal processes acting in the atmosphere, i.e., radiation, condensation, and the eddy flux of sensible and latent heat from the earth's surface. In the present work, a scheme was constructed for the numerical computation of radiative temperature change suitable for incorporation into an advanced general circulation model.

In order to ascertain provisionally the behavior of this scheme, we performed many numerical computations and obtained various distributions of radiative equilibrium temperature as the asymptotic solutions of marching computations from certain initial conditions. In spite of the extreme simplicity of the model, this approach appeared to be very effective for obtaining insight into the role of the radiative processes in maintaining the observed atmospheric temperature distributions.

Theoretical study of the radiative equilibrium of the atmosphere started just after the discovery of the tropopause by Teisserenc de Bort and Assman in 1902. The pioneer theories were those of Humphreys [24], Gold [19], and Emden [12], which were based upon the assumption of gray radiation. Emden computed the vertical distribution of radiative equilibrium temperature as the balance between the heating due to the absorption of solar radiation by water vapor and the cooling due to the long wave radiation of water vapor. His result showed a nearly isothermal layer above the level of 6–8 km. supposedly corresponding to the stratosphere. Below this level there existed the layer of superadiabatic lapse rates which could cause strong convection and corresponds to the troposphere.

This was a successful first step in the study of this field. However, the water vapor absorptivity of terrestrial radiation adopted by Emden, under the assumption of gray radiation, is very different from that obtained by many authors from observations and laboratory experiments. Möller [39] pointed out this difference and recomputed the radiative equilibrium by subdividing the water vapor spectrum into two intervals. His revised computation shows a very low stratospheric temperature approaching -137° C. at the top of the atmosphere and a lapse rate of 0.3° C./100 m. in the stratosphere instead of the isothermal layer obtained by Emden. Based upon these results, he concluded that it is impossible to explain the temperature distribution of the stratosphere by a radiative equilibrium computation including only the effect of water vapor. More recently, King [33] and Yamamoto [71] computed the line absorbing atmosphere in which the absorption coefficients were given by Lorentz's collision broadening formula and Elsasser line shape respectively. Neither of these results shows the inversion in the stratosphere. Although Kaplan [31] obtained the inversion by schematically interpolating the King results, this schematic interpolation seems to be ambiguous.

On the other hand, Gowan [22] computed the distribution of radiative equilibrium temperature of the stratosphere and obtained an *increase* of temperature with altitude by taking into consideration the heating due to the absorption of solar ultraviolet radiation by ozone as well as the effect of long wave radiation by water vapor. In the improved version of his computation [23] he also included the effects of the 15μ band of carbon dioxide, the 9.6μ band of ozone, and the absorption of solar radiation by water vapor. The equilibrium temperature of the stratosphere thus obtained increases with altitude and qualitatively coincides with observed features. Quantitatively, however, the temperatures are much warmer than those observed. This computation could be further improved by adopting recent observations of the extra-terrestrial solar spectrum and the distribution of gases in the stratosphere as well as the absorptivities recently obtained in the laboratory.

The explanation of the temperature increase in the lower stratosphere with increasing latitude is also a difficult task. Möller [40] presented the theory that the overlapping of the ozone band at 14μ and the carbon dioxide band at the same wavelength might be responsible for this increase. As the total amount of ozone increases with increasing latitude, its sheltering effect also increases and a smaller part of carbon dioxide emission leaves the atmosphere. Accordingly, the temperature of the stratosphere could increase with increasing latitude. Quantitatively speaking, however, the intensity of the 14μ band of ozone is much too weak to cause the observed sharp increase of temperature with latitude.

In 1946, Dobson, Brewer, and Cwiling [10] presented a theory of radiative equilibrium which considered the effect

of the 9.6μ band of ozone and the 15μ band of carbon dioxide as well as the long wave radiation by water vapor. In this paper, they beautifully explained the latitudinal distributions and seasonal variation of stratospheric temperature based mainly on the distributions of ozone. Though the 9.6μ band of ozone is much stronger than the 14μ band of ozone, and might have significant effects, the discussion was qualitative and somewhat unverified.

On the other hand, Goody [20] presented a theory which seems to be rather contradictory to the ideas of Dobson's group. He insists that the effect of ozone is of minor importance and explained the latitudinal variation of the tropopause height and of the temperature as a balance between the heating effect of carbon dioxide and the cooling effect of water vapor.

More recently, Ohring [48] computed the radiative heat balance of the stratosphere and concluded that the radiative processes tend to heat the stratosphere in lower latitudes and cool it in higher latitudes. The remarkable differences among the results of these authors suggest the necessity of careful examination of these results as well as quantitative studies of the thermal equilibrium and the heat balance of the atmosphere.

In the present work we took into consideration the effects of the absorption of solar radiation by water vapor, carbon dioxide, and ozone as well as those of the long wave radiation of these three gases. With the aid of recent information on the distributions and absorptivities of these gases, we then computed the distribution of equilibrium temperature for various latitudes and seasons. In addition, in order to investigate the degree of radiative imbalance in observed conditions, the distribution of radiative heat budget was also computed. Based upon these results and the examination of the results of other authors, we tried to determine to what degree we could explain the temperature distribution of the atmosphere by radiative processes and what we should attribute to thermal processes other than radiation, e.g., heat transfer due to large scale disturbances, to the meridional circulation, and to dry or moist convection in the atmosphere.

In recent years, various speculations on the general circulation of the upper troposphere and stratosphere have been inferred from the distribution of the gases such as ozone and water vapor and of radioactive debris introduced into the high atmosphere by atomic explosions (Machta [38]). It is therefore hoped that the comparison of present results with these speculations will shed some light in understanding the thermal processes of the atmosphere.

2. TEMPERATURE CHANGE DUE TO LONG WAVE RADIATION

The absorption bands which mainly contribute to the long wave radiation of the atmosphere are the 6.3μ band and the rotation band of water vapor, the 15μ band of carbon

dioxide, and the 9.6μ band of ozone. The rate of the resultant change of temperature at height z due to the long wave radiation is

$$\left(\frac{\partial T_z}{\partial t}\right)_{LR}^G = -\frac{1}{c_p \rho} \frac{\partial F_z^G}{\partial z} \quad (1)$$

where subscript LR is the abbreviation of long wave radiation, superscript G stands for water vapor (W), carbon dioxide (C), or ozone (O), c_p is the specific heat of air under constant pressure, ρ is the density of air, and the net flux F_z^G is the difference of upward and downward flux, for each wave number interval chosen i.e.,

$$F_z^G = U_z^G - D_z^G. \quad (2)$$

Adding the contribution of the above mentioned three gases, we get the total rate of temperature change due to the long wave radiation as

$$\left(\frac{\partial T_z}{\partial t}\right)_{LR} = \left(\frac{\partial T_z}{\partial t}\right)_{LR}^W + \left(\frac{\partial T_z}{\partial t}\right)_{LR}^C + \left(\frac{\partial T_z}{\partial t}\right)_{LR}^O. \quad (3)$$

Next, we shall describe how we computed the net flux due to these gases. By solving the equation of radiative transfer with the boundary condition that downward long wave radiation is zero at the top of the atmosphere and adopting the method of integration by parts we can express the downward flux of radiation at height z due to any absorption band as

$$D_z = \int_{\nu_1}^{\nu_2} \pi B_\nu(T_z) d\nu - \int_{\nu_1}^{\nu_2} \pi B_\nu(T_\infty) \cdot \tau_f(\chi_\infty) d\nu + \int_{\nu_1}^{\nu_2} \left\{ \int_{T_z}^{T_\infty} \pi \frac{dB_\nu}{dT} \tau_f(\chi) dT \right\} d\nu \quad (4)$$

where $B_\nu(T)$ is the blackbody radiation of frequency ν at temperature T , τ_f is the transmission function of the slab, ν_1 and ν_2 are the band limits, T_z and T_∞ are the temperature at level z and at the top of the atmosphere respectively, and

$$\chi(T) = \left| \int_{u(T_z)}^{u(T)} k_\nu du \right|, \quad (\chi_\infty = \chi(T_\infty)). \quad (5)$$

In equation (5), k_ν is the absorption coefficient at frequency ν , and $u(T)$ is the amount of absorber existing between the earth's surface and the level of temperature T . Assuming that the upward radiation at the earth's surface is equal to the blackbody radiation of surface temperature, we could obtain the upward flux of atmospheric radiation at height z in the same way, i.e.,

$$U_z = \int_{\nu_1}^{\nu_2} \pi B_\nu(T_z) d\nu + \int_{\nu_1}^{\nu_2} \left\{ \int_{T_s}^{T_z} \pi \frac{dB_\nu}{dT} \tau_f(\chi) dT \right\} d\nu \quad (6)$$

where T_s is the temperature of the earth's surface.

Exact integration of equations (4) and (6) requires a

tremendous amount of computation. Therefore, an attempt was made to simplify these equations. The absorption bands of water vapor cover almost the entire spectrum of atmospheric radiation, whereas those of carbon dioxide and ozone have rather narrow band widths. Accordingly, there are some differences between our approximations adopted for the computation of long wave radiation by water vapor and those adopted for the computation for carbon dioxide and ozone. For the sake of convenience we shall describe them separately hereafter.

WATER VAPOR

In order to simplify the computation of equations (4) and (6) Yamamoto [68] introduced the following mean transmissivity of slab:

$$\tilde{\tau}_f(u, T) = \frac{1}{dB} \int_0^\infty \frac{dB_\nu}{dT} \tau_f(k, u) d\nu \quad (7)$$

where

$$\frac{dB}{dT} = \int_0^\infty \frac{dB_\nu}{dT} d\nu. \quad (8)$$

Corresponding to this mean transmissivity of the slab, one can define the mean absorptivity of the slab as

$$\tilde{\epsilon}_f(u, T) = 1 - \tilde{\tau}_f(u, T). \quad (9)$$

The emissivity of the slab of water vapor is by definition

$$\epsilon_f(u, T) = \frac{1}{B(T)} \int_0^\infty B_\nu(T) \cdot \{1 - \tau_f(k, u)\} d\nu \quad (10)$$

where

$$B(T) = \int_0^\infty B_\nu(T) d\nu = \frac{1}{\pi} (\sigma T^4) \quad (11)$$

and σ is the Stefan-Boltzmann constant.

By using $\tilde{\epsilon}_f$ and ϵ_f defined above and neglecting the temperature dependence of k_ν on T , equation (4) could be approximately transformed into the following form:

$$D_z^W \approx \pi B_\infty \cdot \epsilon_f^W(y_\infty, T_\infty) - \int_{B_z}^{B_\infty} \tilde{\tau}_f^W(y, T) \pi dB$$

or referring to equations (7), (9), and (10),

$$D_z^W \approx \pi B_c \cdot \epsilon_f^W(y_\infty, T_c) - \int_{B_\infty}^{B_c} \tilde{\tau}_f^W(y_\infty, T) \pi dB - \int_{B_z}^{B_\infty} \tilde{\tau}_f^W(y, T) \pi dB \quad (12)$$

where

$$y(B(T)) = |u(T) - u(T_z)|, \quad (y_\infty = |u(T_\infty) - u(T_z)|), \quad (13)$$

superfix W corresponds to water vapor, $B_z = B(T_z)$, $B_\infty = B(T_\infty)$, $B_c = B(T_c)$, and T_c is the temperature specially selected for the convenience of integration. Ex-

amination of the table of $\tilde{\tau}_f^W (= 1 - \tilde{\epsilon}_f^W)$ constructed by Yamamoto [68] for the wide range of temperature reveals that $\tilde{\epsilon}_f^W$ is almost independent of temperature for the temperature range of 200°–300°K., i.e., for the range of atmospheric temperature. Below 200°K. it decreases significantly with decreasing temperature. Therefore, if we choose T_c larger than 200°K., we may safely assume that $\tilde{\epsilon}_f^W$ is independent of temperature. For our computation we adopted 220°K. as T_c . Accordingly, ϵ_f^W and $\tilde{\tau}_f^W$ were computed for $T=220^\circ\text{K.}$ and $T=300^\circ\text{K.}$ respectively. For further details of this computation refer to Section 4.

The equation (6) for the upward flux is to be transformed into the following equation:

$$U_z^W = \pi B_s - \int_{B_z}^{B_s} \tilde{\tau}_f^W(y, T) \pi dB \quad (14)$$

where $B_s = B(T_s)$. When the sky is clear, it is more convenient to use the following expression for net flux F_z^W .

$$F_z^W = U_z^W - D_z^W = \pi B_s - \pi B_c \cdot \epsilon_f^W(y_\infty, T_c) - \int_{B_\infty}^{B_s} \tilde{\tau}_f^W(y, T) \pi dB - \int_{B_c}^{B_\infty} \tilde{\tau}_f^W(y_\infty, T) \pi dB. \quad (15)$$

CARBON DIOXIDE AND OZONE

For the 15 μ band of carbon dioxide and the 9.6 μ band of ozone, the mean slab absorptivity of the band instead of that of the entire spectrum was introduced, i.e.,

$$\mathcal{E}_f(u, T) = \frac{1}{\nu_2 - \nu_1} \int_{\nu_1}^{\nu_2} [1 - \tau_f(k, u)] d\nu. \quad (16)$$

Because the band width of these bands is narrow enough to neglect the dependence of dB_ν/dT upon the wave number inside the band, equations (4) and (6), which express the downward and upward radiation respectively, could be changed into the following approximate forms:

$$D_z^G \approx \pi b_\infty^G \cdot \mathcal{E}_f^G(y_\infty, \bar{T}) - \int_{b_z^G}^{b_\infty^G} \mathcal{E}_f^G(y, \bar{T}) \pi db^G \quad (17)$$

$$U_z^G \approx \pi b_s^G - \int_{b_z^G}^{b_s^G} \mathcal{E}_f^G(y, \bar{T}) \pi db^G \quad (18)$$

where superscript G stands either for carbon dioxide or for ozone, \bar{T} is the temperature of isothermal layer which has the same mean band absorptivity and the same distribution of gas as the layer with which we are concerned, b^G is defined as:

$$b^G(T) = \int_{\nu_1^G}^{\nu_2^G} B_\nu(T) d\nu \quad (19)$$

and b_∞^G , b_z^G and b_s^G are the abbreviations of $b^G(T_\infty)$, $b^G(T_z)$,

and $b^G(T_s)$ respectively. Subtracting D_z^G from U_z^G , the net flux F_z^G is

$$F_z^G = \pi b_s^G - \pi b_\infty^G \mathcal{E}_f^G(y_\infty, \bar{T}) - \int_{b_s^G}^{b_\infty^G} \mathcal{E}_f^G(y, \bar{T}) \pi db^G. \quad (20)$$

PRESSURE AND TEMPERATURE EFFECT

Owing to the pressure broadening of line shape the mean absorptivity is also a function of pressure of the layer with which we are concerned. Therefore, it is necessary to take into consideration this effect. Recently, Howard, Burch, and Williams [27] measured the mean absorptivity due to each absorption band of both water vapor and carbon dioxide for various absorber concentrations and various total pressures. According to their results, the mean absorptivity of the layer with uniform pressure could be obtained from the mean absorptivity curve for standard pressure by replacing the optical thickness of the layer u by the effective optical thickness of the layer u_r expressed by the following equation:

$$u_r = \left((P+p)/P_0 \right)^\kappa u \quad (21)$$

where κ is the constant which is usually smaller than unity and is different for each absorption band, P is the total pressure, p is the partial pressure of the absorbing gas, and P_0 is the standard pressure. As is well known, the actual absorption band is the mixture of strong lines and weak lines. When the intensity of a line is very weak or an absorbing gas is very thin, the amount of absorption is proportional to the product of line intensity and the amount of gas and is independent of pressure. This is the reason why κ is usually smaller than 1, despite the fact that a half-width of the line is proportional to pressure.

Strictly speaking, κ is not constant and depends upon amount of absorbing gas and pressure. When the amount of gas is small, κ decreases significantly with decreasing amount of the gas. However, since the thickness of each layer adopted for our numerical computation is thick enough, the assumption of constant κ does not cause serious error. It would be desirable, of course, to adopt a better approximation as soon as more accurate experiments for a wider range of pressure are available.

Since pressure decreases with altitude and $P \gg p$ in the actual atmosphere, the following equation was adopted for the computation of the effective optical thickness of the atmospheric layers instead of equation (21).

$$u_r \approx \int_{u(P_1)}^{u(P_2)} (P/P_0)^\kappa du \quad (22)$$

where, for example, $u(P_1)$ is the optical thickness between the level of total pressure P_1 and the earth's surface. As pointed out by Kaplan [31] linear scaling tends to overestimate the pressure effect for the moderately weak

lines. In this paper, we shall consistently adopt this κ scaling instead of linear scaling.

Temperature also affects the intensity as well as the half width of the absorption lines. However, as far as we know, no suitable measurement has yet been made below room temperature. According to the theoretical estimation of Plass [50, 51], temperature hardly affects the absorption due to the 9.6μ band of ozone but is rather important for the absorption of the 15μ band of carbon dioxide. Therefore, the temperature dependence on absorptivity of the 15μ band of carbon dioxide was incorporated into our computation of heat balance. For the sake of convenience of description, the detailed method of doing this will be described in section 4.

OVERLAPPING

So far we have treated the contributions of the absorption bands of the various gases interdependently; however, the effect of overlapping among these bands deserves attention. The overlapping between the 9.6μ band of ozone and the absorption band of water vapor is not important except near the equator where water vapor is abundant, because water vapor is almost transparent for the radiation of this wavelength. On the other hand, the effect of overlapping between the 15μ band of carbon dioxide and the rotation band of water vapor is not negligible. The mere addition of the contributions of these two gases could give us a fictitious resultant emissivity which is larger than 100 percent. In our computations we made the approximation that water vapor is completely transparent for this overlapped frequency range. In the lower troposphere this approximation would probably be no better than Elsasser's [11] approximation based upon the assumption of complete blackness of the overlapped frequency range. However, in the upper troposphere and stratosphere, where the mixing ratio of water vapor is small and accordingly the absorption by the overlapped range of the rotation band of water vapor is small, the present approximation should be accurate. In order to obtain good accuracy everywhere it would be desirable to adopt the following approximate equation for the resultant slab absorptivity of the overlapped band, $\mathcal{E}_f^{ov}(u^w, u^c)$ (Yamamoto [68]),

$$\begin{aligned} \mathcal{E}_f^{ov}(u^w, u^c) &\approx 1 - (1 - \mathcal{E}_f^{wov}(u^w)) \cdot (1 - \mathcal{E}_f^c(u^c)) \\ &= \mathcal{E}_f^c(u^c) + \mathcal{E}_f^{wov}(u^w) (1 - \mathcal{E}_f^c(u^c)) \end{aligned} \quad (23)$$

where \mathcal{E}_f^{wov} is the mean slab absorptivity of water vapor for the overlapped frequency range. Our approximations correspond to the neglect of the second term on the right side of equation (23).

3. TEMPERATURE CHANGE DUE TO THE ABSORPTION OF SOLAR RADIATION.

The absorption of solar radiation by water vapor, carbon dioxide, and ozone was included in our computa-

tion. If we neglect the effect of overlapping among the absorptions of different gases, the equation for the rate of temperature change at height z due to these absorptions is

$$\left(\frac{\partial T_z}{\partial t}\right)_{SR} = \left(\frac{\partial T_z}{\partial t}\right)_{SR}^W + \left(\frac{\partial T_z}{\partial t}\right)_{SR}^C + \left(\frac{\partial T_z}{\partial t}\right)_{SR}^O \quad (24)$$

where $(\partial T_z/\partial t)_{SR}^W$, $(\partial T_z/\partial t)_{SR}^C$, and $(\partial T_z/\partial t)_{SR}^O$ are the rates of temperature change due to water vapor, ozone, and carbon dioxide respectively, and subscript SR is the abbreviation of solar radiation. The rate of temperature change at height z due to each gas is

$$\left(\frac{\partial T_z}{\partial t}\right)_{SR}^G = -\frac{\cos \xi}{c_p \cdot \rho} \cdot \frac{\partial}{\partial z} \left[a^G \{ (u_\infty - u_z) \sec \xi \} \right] \quad (25)$$

where a^G is the amount of absorption of solar radiation as the function of optical thickness, and ξ is the zenith distance of the sun. In order to compute the equilibrium temperature of the atmosphere, it is necessary to get the expression for the rate of daily mean temperature change. The daily mean rate of temperature change at height z due to the absorption of solar radiation by gas G is

$$\overline{\left(\frac{\partial T_z}{\partial t}\right)_{SR}^G} = \frac{1}{(\text{whole day})} \left[-\frac{\cos \xi}{c_p \rho} \int \frac{\partial}{\partial z} [a^G \{ (u_\infty - u_z) \sec \xi \}] dt \right] \quad (26)$$

which could be approximately expressed as

$$\overline{\left(\frac{\partial T_z}{\partial t}\right)_{SR}^G} \approx \frac{(\text{daytime})}{(\text{whole day})} \left[-\frac{\cos \bar{\xi}}{c_p \cdot \rho} \frac{\partial}{\partial z} [a^G \{ (u_\infty - u_z) / \cos \bar{\xi} \}] \right] \quad (27)$$

where $\bar{\xi}$ is the mean zenith angle defined in the following way:

$$\cos \bar{\xi} = \left(\int \cos \xi(t) dt \right) / \left(\int dt \right) \quad (28)$$

The mean cosine of the zenith angle and the length of daytime given in parts of 24 hours for each season and latitude, which are used in our computation, are tabulated in table 1.

TABLE 1.—The seasonal and latitudinal distributions of the length of the daytime given in parts of 24 hours and those of the weighted mean values of $\cos \xi$. (See table 6 of [36].)

°Lat.	Fractional length of daytime				Cos $\bar{\xi}$			
	Apr.	July	Oct.	Jan.	Apr.	July	Oct.	Jan.
5	.508	.517	.500	.496	.625	.587	.614	.591
15	.521	.537	.492	.471	.618	.601	.579	.549
25	.533	.562	.483	.450	.599	.593	.524	.474
35	.546	.596	.471	.421	.558	.567	.458	.393
45	.562	.637	.454	.362	.501	.521	.379	.317
55	.596	.708	.437	.321	.423	.453	.282	.203
65	.629	.837	.404	.203	.345	.369	.176	.106
75	.750	1.000	.329	----	.241	.311	.071	----
85	1.000	1.000	----	----	.168	.318	----	----

The effect of pressure broadening of the absorption lines was taken into consideration in the same way as for the long wave radiation. The values of κ which should be adopted for the absorption of solar radiation by each gas will be discussed later.

There is an overlapping between the 2.7μ band of water vapor and that of carbon dioxide. In the lower troposphere where the water vapor is abundant, the mere addition of these two contributions causes an over-estimation of the absorption of solar radiation by this band. However, in the troposphere the relative magnitude of the absorption by carbon dioxide is so small that it does not matter whether we include this effect of overlapping or not. For the sake of simplifying the computation scheme, we add the contributions of two gases neglecting the effect of this overlapping.

4. ABSORPTIVITIES OF LONG WAVE RADIATION

In order to compute the temperature change due to the long wave radiation of the atmosphere, it is necessary to know the emissivity or the absorptivity of diffuse radiation. In the laboratory, however, the absorptivity of the parallel beam is usually measured. Therefore, it is necessary to obtain the relation between the absorptivity of a column and that of a slab. For this purpose Elsasser [11] computed the transmissivities of both a slab and a column for an idealized band of equal and equidistant lines. Based upon these results, he obtained the following approximate relation.¹

$$\tau_f^E(l, u) \approx \tau_f^E(1.66l, u) \quad (29)$$

where τ_L^E and τ_f^E are the general transmission function of a column and a slab for this idealized Elsasser band, and l is the general absorption coefficient. This equation means that the effective optical thickness for isotropic diffuse radiation is 1.66 times larger than that for direct radiation. In this section we shall use this approximate relation for the reduction of the absorptivity of a slab from that of a column.

WATER VAPOR

An extensive study of the absorption bands of water vapor contributing to the terrestrial radiation was done by Yamamoto [68]. He obtained the value of the general absorption coefficient for the 6.3μ band, $8-13\mu$ region, $17-24\mu$, and the far infrared region from the experiments by Fowle [16], Adel and Lampland [1], Weber and Randall [66], and the theoretical computations of Yamamoto and Onishi [67], respectively. According to his paper, the theoretical computation by Yamamoto and Onishi coincides well with the experimental results by Weber and Randall for the rotation band at $17-24\mu$ but does not coincide with the experiments by Fowle for the rotation vibration band at 6.3μ , due probably to the crude approximation adopted in their theoretical computation for this

¹ This kind of approximation was first adopted by Robert [54].

band. Recently, careful and extensive experiments on this band were performed by Howard, Burch, and Williams [27] which coincide very well with the results of Fowle. This coincidence supports Yamamoto's choice of Fowle's experimental data for this band.

By using the general absorption coefficients for 300° K. and 220° K. and the general transmission function compiled by Yamamoto [68], we computed the mean slab absorptivity $\tilde{\epsilon}_f(u^w, 300^\circ \text{K.})$ and slab emissivity $\epsilon_f(u^w, 220^\circ \text{K.})$, respectively, which are given in figure 1 for the logarithm (base 10) of varying optical thicknesses in the unit of centimeter of precipitable water. The contribution of the frequency range overlapped with the 15 μ band of carbon dioxide (550–800/cm.) was not included in this computation.

The value of the pressure factor κ for the absorption bands of water vapor could be obtained from the experiments performed by Howard et al. [27] and Daw [9]. Howard et al. conducted laborious experiments on many infrared absorption bands of water vapor and carbon dioxide and proposed two types of relations which fit the experimental data. When the absorption is weak, the total absorption is given by the following equation of "weak fit":

$$\int_{\nu_1}^{\nu_2} A_\nu d\nu = C \{u (P+p)^\kappa\}^{1/2} \text{ (weak fit)}^2. \quad (30)$$

For the stronger absorption the total absorption is given by the following equation of "strong fit":

$$\int_{\nu_1}^{\nu_2} A_\nu d\nu = C + D \log_{10} \{u (P+p)^\kappa\} \text{ (strong fit)}^2. \quad (31)$$

In table 2 the values of κ for the 6.3 μ band and the rotation band are tabulated both for the strong and for the weak fit. Referring to this table, we assumed the effective mean κ -value for both the rotation band and the 6.3 μ band to be 0.6.

In view of the fact that Daw's experiments do not cover the entire rotation band of water vapor and that the theoretical computation of line intensity of the rotation band is possible, it seems desirable to determine the κ -value for the rotation band based upon the theoretical computation. Before this sort of computation is done, we tentatively adopt the κ -value of 0.6.

CARBON DIOXIDE

Careful study of the absorptivity of the 15 μ band of carbon dioxide was made by Howard, Burch, and Williams [27] for absorber concentration ranging from 1 to at least 1000 atmo-cm. of carbon dioxide and for various

² According to Benedict [4], the collision cross section of H₂O–N₂ collision is 6–7 times as large as that of N₂–N₂ collision instead of twice implied by equations (30) and (31). If so, reanalysis of the experiment by Howard et al. [27] seems to be desirable. Before this is done, we shall tentatively adopt their present results.

TABLE 2.—The value of κ for rotation band and 6.3 μ band of water vapor*

Band	Band Limits (cm. ⁻¹)	κ	Reference
Rot H ₂ O.....	436-655	0.60 (weak fit)...	Daw [9]*.
Rot H ₂ O.....	655-896	.50 (weak fit).....	Daw [9]*.
6.3 μ	1150-2050	.60 (weak fit).....	HBW [27].
		.72 (strong fit).....	HBW [27].

*The κ -values for the rotation band were taken from p. 16-12 of the *Handbook of Geophysics* [18], where King gave the value of κ and other constants based upon Daw's data.

total pressures ranging from 20 mm. to 740 mm. Hg. They expressed their results by the equations of weak and strong fit as they did for the absorptivity of water vapor (refer to equations (30) and (31)). By using these empirical equations it is possible to construct the curve of the mean band absorptivity of a slab for the 15 μ band of carbon dioxide.

According to their experiment, the pressure factor κ for a weak fit is 0.855 and that for a strong fit is 0.88. Based upon these values we assumed κ to be 0.86.

The dependence of absorptivity of this band on temperature is not always small. This was pointed out, for example, by Plass [51]. In order to calculate the temperature effect, we used the recent work of Sasamori [55] who theoretically computed the absorptivity of this band

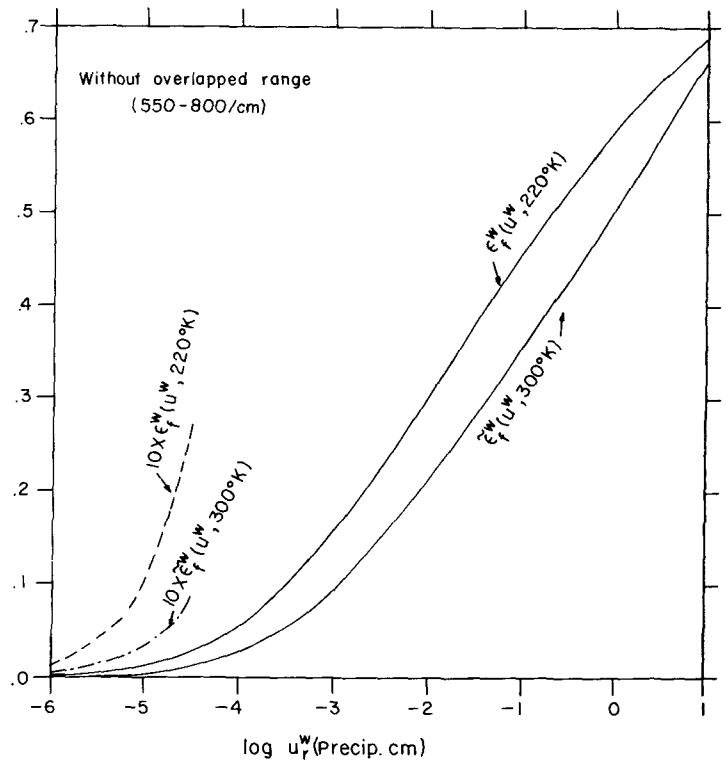


FIGURE 1.—The slab emissivity and the mean slab absorptivity of water vapor. The contribution of the frequency range overlapped with the 15 μ band of carbon dioxide (550–800/cm.) was not included.

for various temperatures. Though his theoretical curve at normal temperature and 1 atmosphere pressure (NTP) does not exactly coincide with the experimental curve mentioned above [27], his results give us the approximate magnitude of the change of effective optical thickness corresponding to the change of temperature. By shifting horizontally the experimental curve mentioned above by the same distance³ as the distances between the curve at 300° K. and that at other temperatures shown in figure 2 of Sasamori's paper, the final absorption curves were obtained for various temperatures which are shown in figure 2 and were used for our computation. Interpolation of these curves in this figure gives us the approximate absorptivity curve for any temperature above 218° K. and below 300° K. When the temperature is higher than 300° K. or lower than 218° K. we adopt the absorptivity of 300° K. and 218° K., respectively. In order to use these absorptivities, it is necessary to compute the effective temperature of the atmospheric layers. Although the mixing ratio of carbon dioxide is approximately constant with height, pressure as well as temperature vary with altitude. Therefore, the estimation of effective temperature involves cumbersome computations. (See, for example, Plass [51]). In view of the fact that the absorptivity of carbon dioxide at NTP is itself subject to some uncertainty, we adopted the following simplest possible approximation for the computation of effective temperature T_{eff} .

$$T_{eff} = \left(\int_{P_1}^{P_2} T dP \right) / \left(\int_{P_1}^{P_2} dP \right) \quad (33)$$

where P_1 and P_2 are pressures of upper and lower limits of the layer, respectively. After obtaining this effective temperature, we can compute the absorptivity of the layer for T_{eff} by linearly interpolating absorptivities with respect to temperature.

This effect of temperature on the absorptivity of the 15 μ band of carbon dioxide was included in the computation of the heat balance of the atmosphere but, for the sake of simplicity, not in the computation of radiative equilibrium. In the latter computation, we adopted the absorptivity at 218° K. consistently.

OZONE

Laboratory measurements of the absorptivity of this band were made by Summerfield [60] and more recently by Walshaw [65]. The latter experiments were used for our purpose. In his paper, Walshaw presents empirical expressions which agree well with the observed absorption curve but are at the same time quite complicated.

In this study, for the sake of simplicity, his data were re-analyzed to get the absorptivity suitable for our system of computation. Re-analysis was confined to the runs a-i of Walshaw's experiment which cover the ordinary

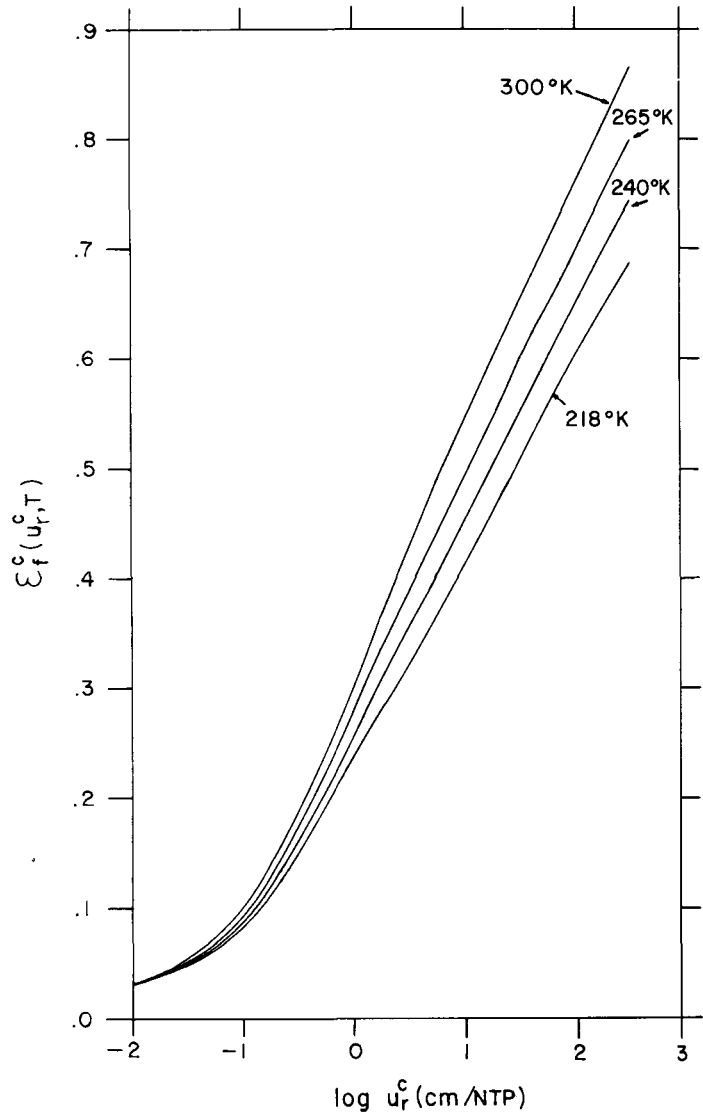


FIGURE 2.—The mean slab absorptivity of the 15 μ band of carbon dioxide for various temperatures. The absorptivity for 300° K. is based on the experiment by Howard et al. [27]. The temperature dependence of the absorptivity was estimated based upon the theoretical computation of Sasamori [55].

range of ozone amounts in the atmosphere. Based upon these runs, the value of κ was determined to be 0.3 by the least squares method.⁴

In figure 3, observed values of mean band absorptivity of a column were plotted versus effective optical thickness u_r which is defined by

$$u_r = [(P + .61p)/P_0]^{.3} u \quad (34)$$

The addition of 0.61 p to the total pressure P , which appears in the numerator of this equation, was originally suggested by Walshaw [65]. Based upon his results of

⁴ In order to perform the least squares method, absorptivity was tentatively assumed to be proportional to the square root of the amount of ozone.

³ Of course, this distance depends upon the amount of CO₂ also.

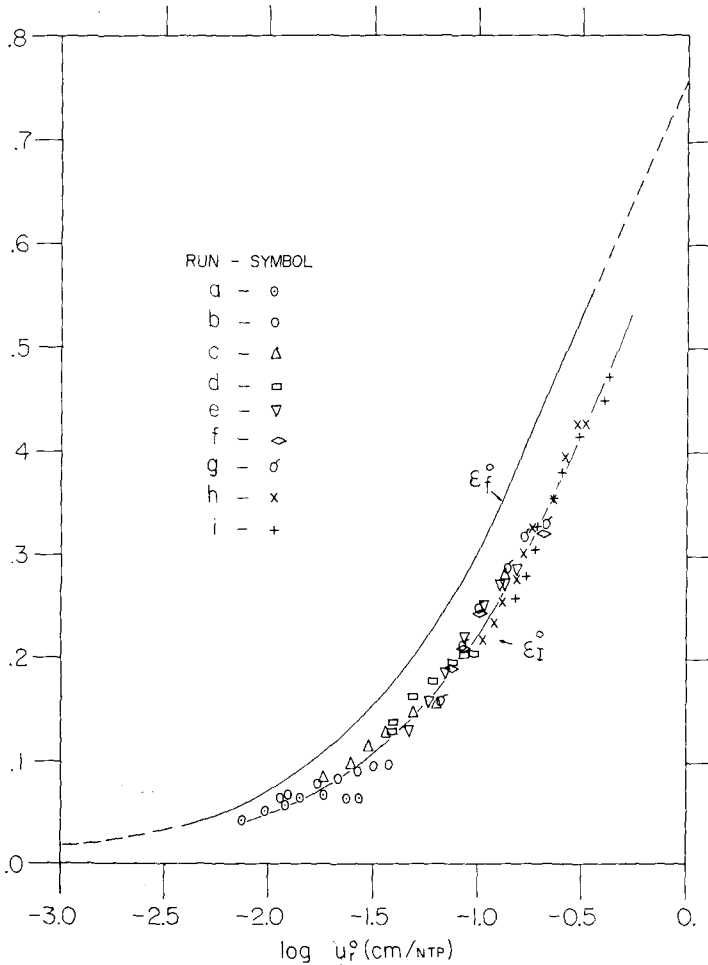


FIGURE 3.—The mean absorptivities of both column and slab of the 9.6μ band of ozone (i.e., \mathcal{E}_c^0 and \mathcal{E}_s^0) obtained by processing the results of Walshaw's experiment [65]. The symbols adopted for plotting his measurement of mean absorptivity of column are the same as those adopted by himself for the series of runs of his experiment.

experiments, he concluded that the effective collision cross section of ozone is about 1.61 times as large as that of air. For the atmospheric condition, however, $P \gg p$, so this addition is not necessary.

The curve of best fit to these data gave us the mean band absorptivity of a column which was changed into the mean band absorptivity of a slab in the usual way. The slab absorptivity corresponding to the logarithm (base 10) of the various effective amounts of ozone (Unit: cm./NTP), which was used for our computation, is also shown in figure 3.

Examining the plotted values in figure 3 carefully, we notice that there is a rather large scattering of points for a small amount of effective ozone. (Refer to runs a, b.) Analyzing Walshaw's experiment for a small amount of ozone we notice the following tendency. As the pressure becomes larger, i.e. approaches 1 atmosphere pressure,

absorptivity seems to become more or less independent of pressure. This small dependence is the cause of scattering of plotted points and suggests the inadequacy of equation (34) for incorporating the pressure dependence. However, as the pressure in or near the ozone layer, where the effect of this band is important, is much less than 1 atmosphere pressure, this tendency should not cause serious error in our computation.

5. ABSORPTION OF SOLAR RADIATION WATER VAPOR

Based mainly upon Fowle's work [14], [15], [16], the absorptivity curve of solar radiation by water vapor has been constructed by Kimball [32], Mügge-Möller [42], Yamamoto-Onishi [69], Houghton [25], and McDonald [37]. For this work, in order to cover the small amount of water vapor, we constructed the absorption curve based mainly upon experiments by Howard et al. [27].

According to their paper [27], the water vapor absorption bands at $6.3, 3.2, 2.7, 1.87, 1.38, 1.1,$ and 0.94μ were studied individually for the absorber concentrations ranging from 0.001 to 3.8 cm. of precipitable water and for the various total pressures with nitrogen up to 740 mm. Hg. Using mainly these results, we obtained the absorption of solar radiation by water vapor. Although Howard et al. did not give the absorption for the amount of precipitable water which is more than 3 cm., they determined the parameter of Goody's random model by use of their experimental results and predicted the magnitude of band absorption for 3, 10, and 50 cm. of precipitable water. Therefore, we can compute the absorption up to 50 cm. of precipitable water. For the absorption by a very small amount of precipitable water which was not covered by their experiments, we simply used the experimental equation for weak fit proposed by Howard et al. [27].

The absorption bands at 0.75 and 0.85μ were not covered by their experiment because of the minor importance of these bands. In view of the fact that the intensity of near infrared solar spectrum increases with decreasing wavelength, the contributions of these two bands are not negligible when the amount of precipitable water is more than 1 cm. Although the absorption band at 0.94μ was covered by their experiment, parameters of

TABLE 3.—The values of κ for various absorption bands of water vapor which absorb solar radiation (after Howard et al. [27]).

Characteristic wavelength (μ)	κ Weak fit	κ Strong fit
6.3	0.60	0.72
3.2	.60	-----
2.7	.64	.61
1.87	.60	.62
1.38	.60	.43
1.1	.52	-----
0.94	.54	-----

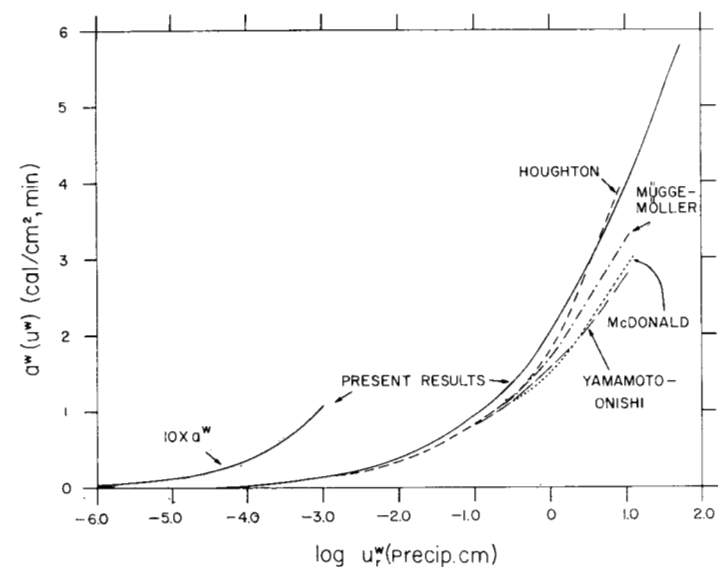


FIGURE 4.—Comparison of the absorption of solar radiation by water vapor by various authors.

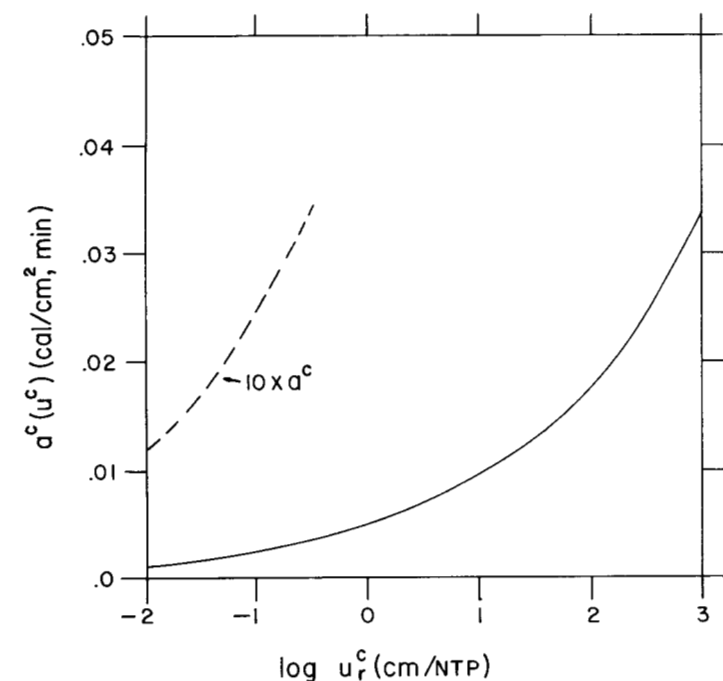


FIGURE 5.—The amount of the absorption of solar radiation by carbon dioxide based upon the results of experiment by Howard et al. [27].

Goody's model were not given, due probably to the poor accuracy of the laboratory experiment for this band. Therefore, their result cannot be extrapolated to the amount of water vapor which is larger than a few cm. of precipitable water.

In order to compute these three weak bands which are of rather minor importance, we used Fowle's data.

Extrapolation of his absorption curve to larger optical thickness was done by using the general absorption coefficient of Yamamoto and Onishi [67]⁵ and the general transmission function of Elsasser band.

Finally, summing the contributions from these 9 bands, we computed the absorption of solar radiation versus the amount of precipitable water, which is shown in figure 4. Also in figure 4 the absorption curves obtained by other authors are shown for the sake of comparison. On the ordinate the rate of absorption is given in units of cal./cm.² min., and on the abscissa logarithm (base 10) of water is given in units of cm. of precipitable water. In order to compare our result with that of McDonald, it is necessary to add the contributions from the absorption bands at 2.7, 3.2, and 6.3 μ to McDonald's curve. If we do that, the difference between our curve and McDonald's or Mügge-Möller's curve is approximately 10 percent.

In spite of the fact that Houghton [25] found some inconsistencies between the Fowle publications and the data published by Smithsonian co-workers, the band absorptivities obtained by Fowle and those by Howard et al. coincide with each other well,⁶ and the difference between our curve and Mügge-Möller's does not seem to cause a serious effect, whichever result is correct.

In order to incorporate the pressure effect properly, it is necessary to find the proper value of κ for those bands. Table 3 shows the values of κ which were obtained by Howard et al. [27] experimentally for both the strong and weak fit. Referring to this table, we assume the value of κ common for all those bands to be 0.6. This value is the same as the κ -value adopted for the terrestrial radiation of water vapor.

CARBON DIOXIDE

Extensive experiments by Howard, Burch, and Williams [27] are available for the computation of the amount of absorption of solar radiation by carbon dioxide. They studied the carbon dioxide absorption bands at 5.2, 4.8, 4.3, 2.7, 2.0, 1.6, and 1.4 μ individually for absorber concentration ranging from 1 to at least 1000 atmo-cm., for various total pressures including nitrogen up to 740 mm. Hg.

Based upon their results and the solar irradiant spectrum outside the earth's atmosphere which is given in the Smithsonian Meteorological Tables, the resultant absorption curve can be constructed by summing the contribution of the 7 bands mentioned above. Figure 5 gives this relation between the absorption of solar radiation (cal./cm.² min.) versus the logarithm (base 10) of the amount of carbon dioxide (cm./NTP).

In order to take into consideration the effect of pressure

⁵ Though their general absorption coefficients were based upon Fowle's data and rather crude theoretical computations, some adjustment of the coefficients was needed to make the resultant absorption curves coincide with Fowle's.

⁶ There is some significant difference in the absorptivities of the 1.38 μ band. Howard's absorptivity is larger than Fowle's.

TABLE 4.— κ -values for various CO_2 bands which absorb solar radiation. $(\bar{A\nu})_{crit.}$ is the upper limit of the mean band-absorptivity for which the equation of weak fit is applicable.

Characteristic wavelength (μ)	κ Weak fit	κ Strong fit	$(\bar{A\nu})_{crit.}$
5.2	0.80	-----	0.273
4.8	.74	-----	.333
4.3	-----	.93	.147
2.7	.86	.88	.156
2.0	.78	.83	.178
1.6	.76	-----	.145
1.4	.82	-----	.133

broadening, it is necessary to know the magnitude of κ . Table 4 gives the values of these 7 absorption bands obtained by Howard, Burch, and Williams for both the strong and the weak fit. The value of κ for the weak fit concentrates around 0.8 and that for the strong fit concentrates around 0.9. Therefore, we assume the value to be 0.86 which is the same as the one used for the computation of long wave radiation of the 15μ band of carbon dioxide.

OZONE

In order to compute the amount of solar radiation absorbed by ozone, it is first necessary to know the ultra-violet portion of the solar spectrum irradiance curve outside the earth's atmosphere. Recent work of Johnson [30] is available for this purpose. He constructed the improved version of the solar irradiance curve outside the atmosphere using recent results of the observations obtained by high altitude rocket as well as the Smithsonian observations.

Another bit of information needed for the construction of the absorption curve is the absorptivity of ozone with respect to various wavelengths. The most recent data about which the authors know are the results of experiments by Vigroux [64] and by Inn and Tanaka [28]. In spite of the distinct differences in the experimental methods, the agreement between them is fairly good.

In this paper, following the recommendation by Inn and Tanaka [29], we used Vigroux's experiment for the computation of the absorption due to Huggins band (3000-3700 Å.) and the experiment by Inn and Tanaka for the computation of the absorption due to the Hartley (2000-3000 Å.) and Chappuis bands (4400-7600 Å.). In view of the temperature of the stratosphere where the absorption due to ozone mainly takes place, we adopted the absorption coefficients for the temperature of $-40^\circ C$. The values could be calculated from the estimate of Vigroux who observed the ozone absorption over the $-92^\circ C$. to $120^\circ C$. temperature range. In figure 6 continuous lines show the total amount of absorption due to ozone (cal./cm.² min.), that due to the Hartley and Huggins bands, and that due to Chappuis band versus the logarithm of the amount of ozone (cm./NTP). For the sake of comparison, the absorption curve which is obtained by integrating the diagram constructed by

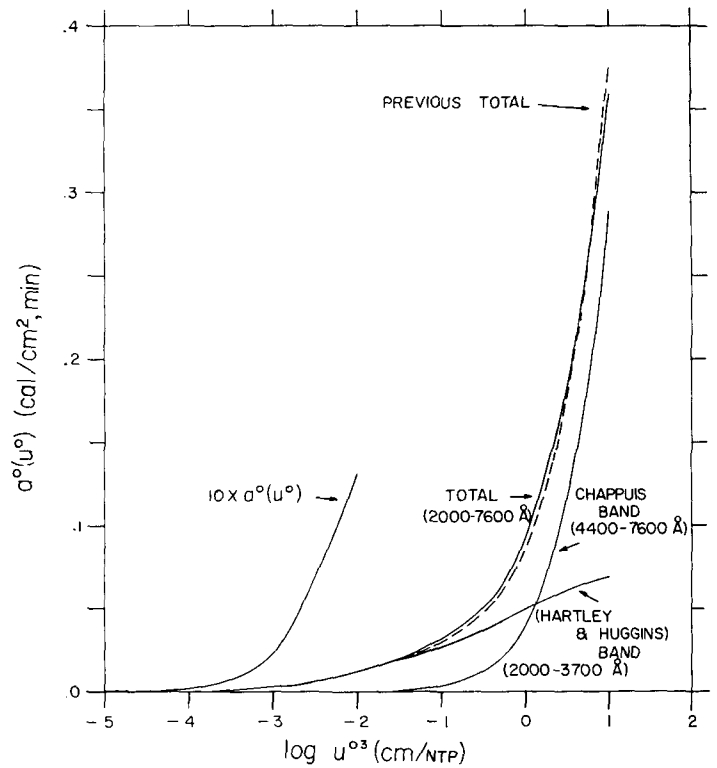


FIGURE 6.—The amount of the absorption of solar radiation by ozone based upon the results of experiments by Vigroux [64], and Inn and Tanaka [28]. The contribution of each band is also shown in the figure.

Craig [8] and extended by Pressman [52] is also shown in figure 6 as a dashed curve. In spite of the fact that the latter curve is based upon the older experiment by Ny and Choong [46, 47], and upon different solar irradiant curves, the coincidence between these two absorption curves is good.

6. DISTRIBUTION OF GASES

WATER VAPOR

The vertical and latitudinal distributions of water vapor in the atmosphere were compiled by Telegadas and London [61] and London [36], based upon surface and radiosonde observations. We adopted their distributions of the relative humidity in the lower half of the troposphere where the temperature is above $-30^\circ C$. and the measurements of relative humidity by radiosonde are accurate enough. In the upper half of the troposphere where the temperature is below $-30^\circ C$. we adopted the constant frost point lapse rate of $-6.25^\circ C/km$. which coincides with the results of many observations from an airplane conducted by the British group [43], [63].

Concerning the moisture distribution at the higher altitude Barclay et al. [2] constructed a convenient figure which shows the results of various authors in compact form and is reproduced in figure 7. Among them, Bar-

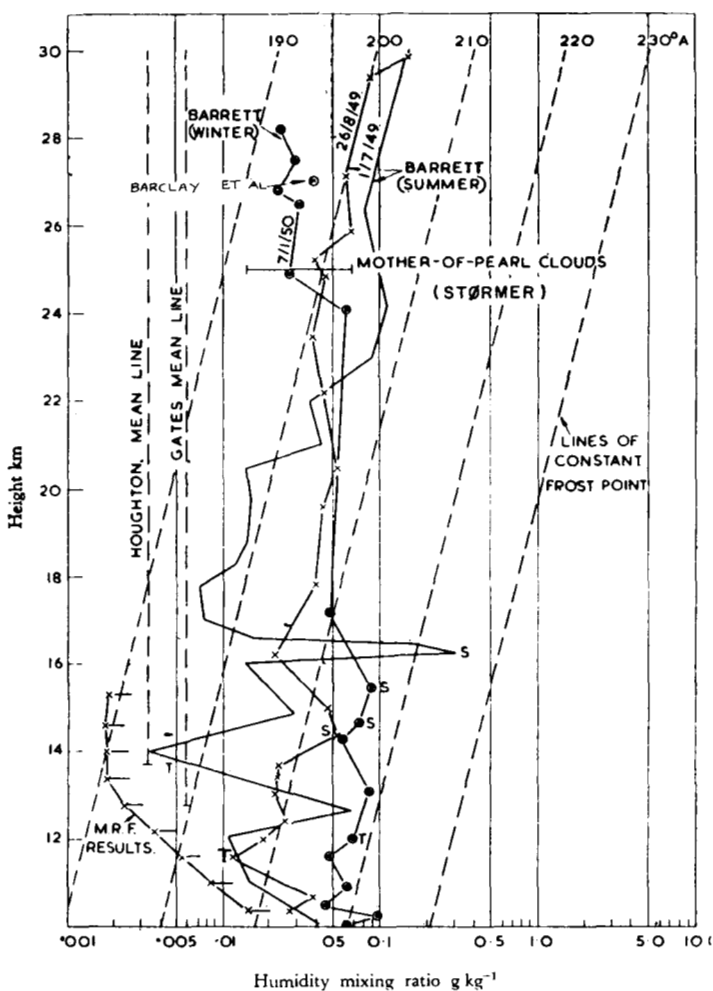


FIGURE 7.—The vertical distributions of water vapor obtained by various authors and compiled by Barclay et al. [2]. The data for mother-of-pearl clouds are from Størmer [59].

rett's [3] results seem to be too large, due probably to the evaporation from the balloon. Therefore, based upon the measurements by Murgatroyd et al. [43] and the infrared measurements by Houghton et al. [26] and Gates et al. [17], we tentatively assumed the constant frost point of 190°K . in the stratosphere up to the height of about 30 km. (9-mb. level) and assumed a constant mixing ratio above this level. This gives the total amount of moisture which is consistent with infrared measurement. The final results of the vertical distribution of moisture which were obtained by the British group, and summarized by Tucker [63], are given in figure 8a. It is very interesting that the frost point decreases with height and approaches the value of about 190°K . irrespective of season. Recently Murgatroyd⁷ obtained his results of the measurements of vertical distribution of water vapor at various latitudes which are also reproduced in figure 8b. According to these results the frost point seems to approach

⁷ Private communication. See reference [44].

almost the same value, i.e. 190°K ., irrespective of latitude. In view of these results our assumption that the frost point is constant in the stratosphere irrespective of season and latitude seems to be reasonable.

In figure 9 the latitudinal and vertical distributions of the mixing ratio (gr./kg. of air) of water vapor for all seasons, which we adopted for our computations, are shown.

CARBON DIOXIDE

It is generally considered that the proportion of carbon dioxide is relatively invariant below 90 km. According to the table presented on page 8-1 of [18] the amount of carbon dioxide is approximately 0.03 percent by volume or 0.0456 percent by weight. The reduced thicknesses of carbon dioxide at normal temperature and normal pressure were computed from these data.

OZONE

The seasonal and latitudinal distribution of ozone was first given by Götz [21] in the form of a diagram. Based upon the more recent measurement of higher sensitivity, Normand [45] improved the diagram by removing the Arctic winter gap which exists in the original case. Normand's diagram must be modified further because the amount of ozone in his diagram was computed by use of the absorptivity of Ny and Choong [46], [47], which is about 36 percent larger than that of Vigroux at the wavelength adopted for this computation. The latitudinal distributions of the total amount of ozone for all seasons are shown in figure 10 in the Vigroux scale.

Concerning the vertical distribution of ozone, Tønsgaard and Olsen [62] found a good correspondence between the total amount of ozone and vertical distribution. Figure 11 shows this correspondence in the Vigroux scale.

From figure 10 and figure 11 it is possible to obtain the distribution of ozone with respect to latitude, season, and height which we used for our computation.

7. COMPUTATION OF RADIATIVE EQUILIBRIUM

So far we have constructed a scheme for the computation of radiative temperature change, deduced the absorptivities from various theoretical and experimental results, and determined the distribution of various atmospheric gases consistent with the observations obtained by various authors. Now we are in a position to compute the seasonal and latitudinal distributions of the radiative equilibrium temperature as well as that of heat balance.

The basic principle of the method of computation is to approach the state of radiative equilibrium asymptotically from certain initial conditions. If we express temperature as a function of height and time, i.e., $T(z,t)$, equilibrium temperature might be expressed by $T(z,\infty)$. Since it is

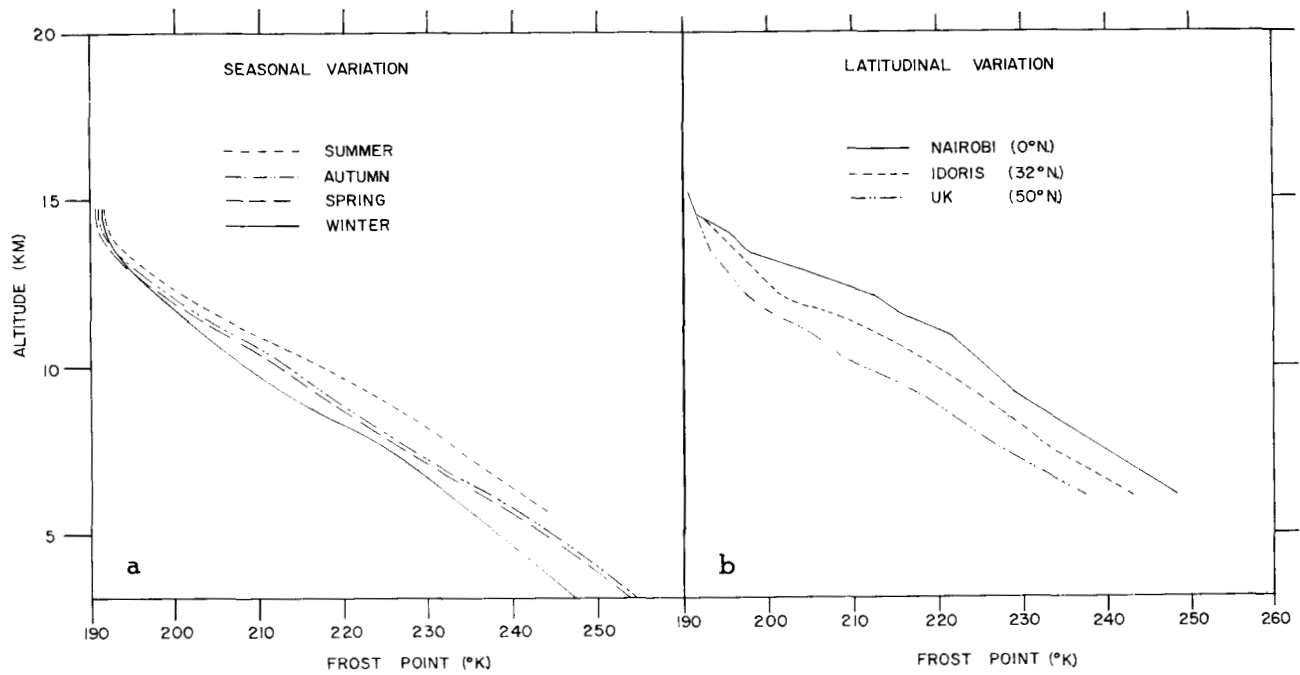


FIGURE 8.—(a) Seasonal variations of the vertical distribution of water vapor which were measured from an airplane by the British group [43] and compiled by Tucker [63]. (b) The vertical distribution of water vapor at various latitudes obtained by Murgatroyd (private communication).

possible to determine the rate of temperature change uniquely from the distributions of temperature and gases, and since the continuous variation of temperature distribution causes continuous variation of the rate of temperature change, there exist such δ and t_c as to satisfy the following condition for any value of \mathcal{E} :

$$\mathcal{E} > \text{Max} |T(z, \infty) - T(z, t_c)| \quad (35)$$

and

$$\delta > \text{Max} \left| \left(\frac{\partial T(z, t_c)}{\partial t} \right)_{\text{RAD}} \right| \quad (36)$$

where

$$T(z, t_c) = T(z, 0) + \int_0^{t_c} \left(\frac{\partial T(z, t)}{\partial t} \right)_{\text{RAD}} dt \quad (37)$$

and

$$\left(\frac{\partial T(z, t)}{\partial t} \right)_{\text{RAD}} = \left(\frac{\partial T(z, t)}{\partial t} \right)_{\text{LR}} + \left(\frac{\partial T(z, t)}{\partial t} \right)_{\text{SR}} \quad (38)$$

In other words, we can approach the radiative equilibrium as closely as we want by properly choosing the magnitude of δ .

In order to perform the integration of equation (37) by a finite difference scheme, we adopted the forward time difference, i.e.

$$T(z, t + \Delta t) = T(z, t) + \left(\frac{\partial T(z, t)}{\partial t} \right)_{\text{RAD}} \Delta t \quad (39)$$

Brunt [5] shows that the equation of temperature change due to atmospheric radiation could be crudely approximated by an equation of heat diffusion. According to Richtmyer [53], the finite difference time integration of a diffusion equation can be performed stably by adopting forward time differencing and choosing the proper time interval. Based upon this information, we used forward time differencing for our integration. The optimum time interval which satisfies the condition of computational stability was determined by a trial and error method. For our grid system (refer to Appendix I) the integration was stable for time intervals shorter than 12 hours but was unstable if we adopted a 24-hour interval. We adopted an 8-hour interval throughout our computations of radiative equilibrium.

The lower and upper computational boundary conditions are

$$T(0, t) = T_s = \text{const.} \quad (40)$$

at the ground surface, and

$$\partial T / \partial p = 0 \quad (41)$$

at the top of the atmosphere. (Refer to equation A-3 in the Appendix III for exact meaning of latter condition).

The initial condition which we adopted for the computation of radiative equilibrium was an isothermal atmosphere with the observed temperature of the earth's surface. Since we adopted a finite value of δ , the final equilibrium temperature has an uncertainty of the order

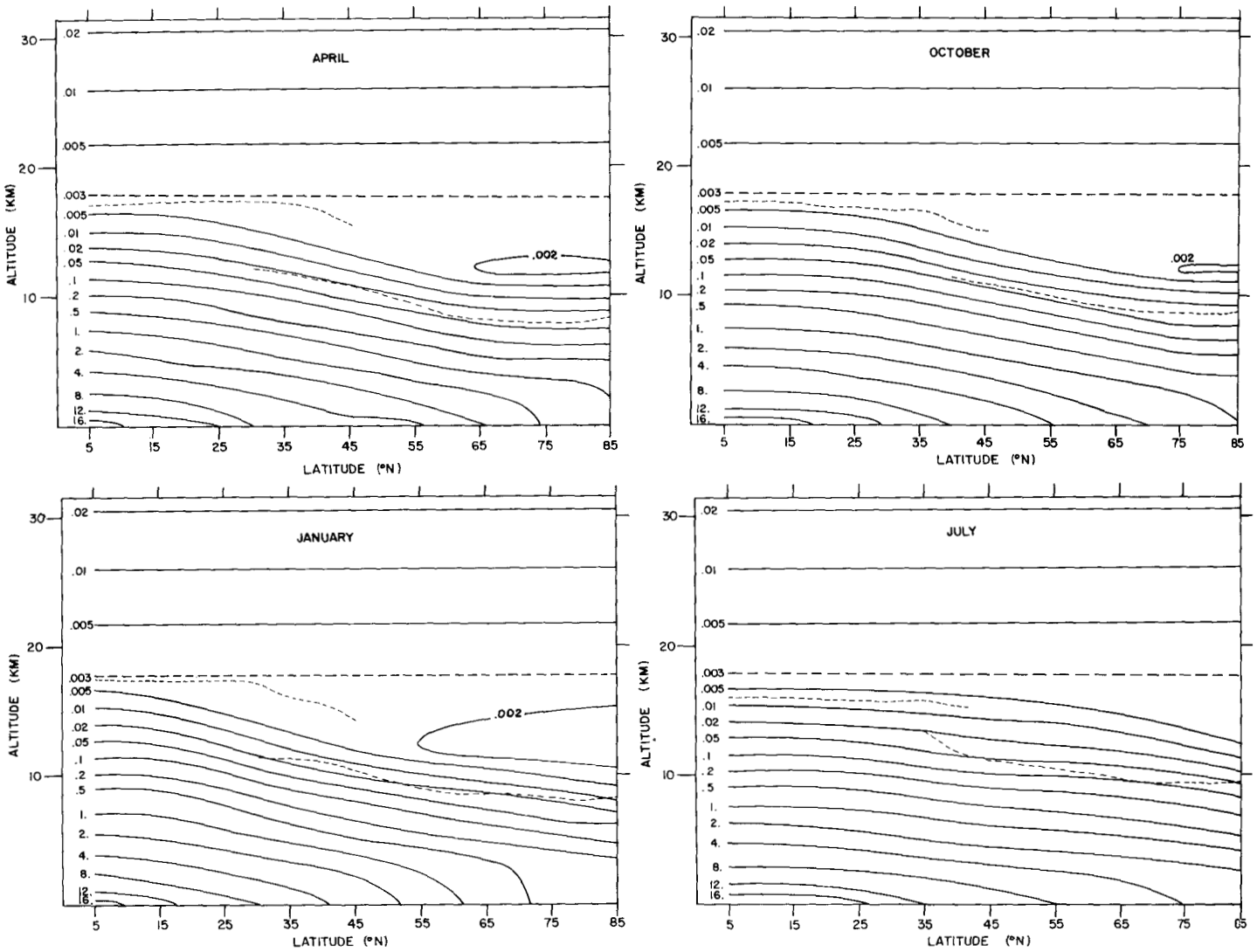


FIGURE 9.—Seasonal and latitudinal distribution of water vapor (g./kg. of air) adopted for our computation. The thin dashed lines show the height of the tropopause determined by Kochanski [34].

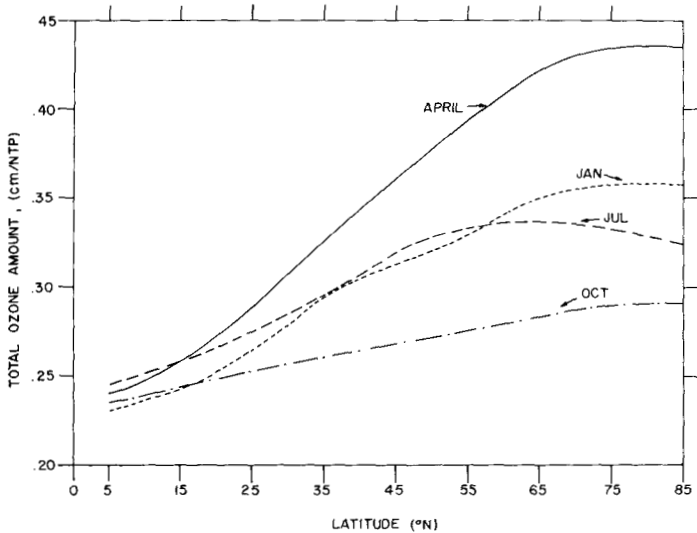


FIGURE 10.—Seasonal and latitudinal distributions of the total amount of ozone compiled originally by Götz [21] and modified later by Normand [45].

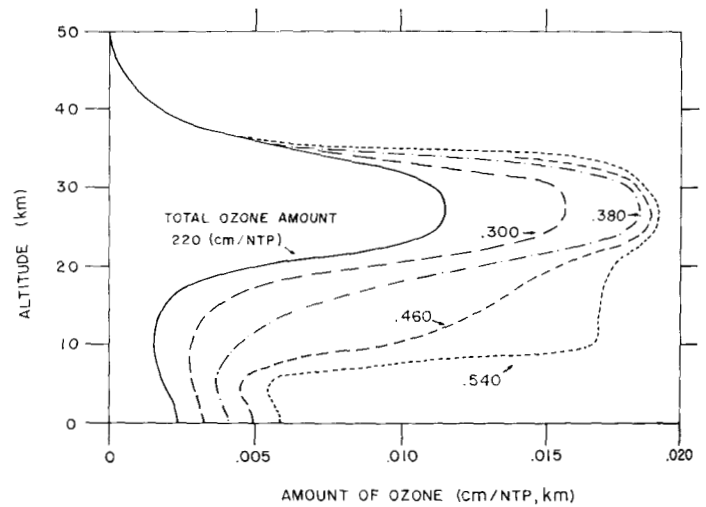


FIGURE 11.—Vertical distributions of ozone corresponding to the various total amounts in the Vigroux scale obtained by Tønsberg and Olsen [62].

of magnitude of \mathcal{E} , depending upon the initial conditions chosen. Therefore, in order to compare our results with each other it is desirable to start from the same initial conditions, which we did. For our computations we adopted values of δ ranging from 0.03°C./day to 0.07°C./day . According to our estimate by extrapolation, the maximum difference between the actual and the computed equilibrium temperatures appears around the tropopause when we adopted the isothermal initial condition and varies⁸ from 3°C. – 7°C. corresponding to the range of δ given above. The time for reaching this quasi-equilibrium state depends upon the amount of sunshine and the magnitude of δ . When we adopt 0.07°C./day for δ , this time ranges from 200 to 500 days, depending upon the amount of sunshine. The weaker the sunshine, the longer it takes to reach this quasi-equilibrium.

Along with the computation of the equilibrium temperature by this initial value method reported in this paper, we also computed it as the solution of a homogeneous set of equations whose unknowns are the temperatures at various levels. The preliminary results obtained by adopting this matrix method are to be published [41]. Using this matrix method, we can get the vertical distribution of equilibrium temperature immediately and are free of the uncertainty, \mathcal{E} , that we have in the initial value method. Therefore, the results obtained by this matrix method serve as an independent check of the present initial value method. In order to adopt this linear matrix method, however, it is necessary to linearize the equation of temperature change with respect to temperature. Whereas for the initial value method it does not matter whether the equation is linear or non-linear with respect to temperature. In this respect the present initial value method is much more flexible and more accurate than the matrix method. The initial value method might be regarded as one of the methods for solving the set of non-linear equations by successive approximation.

8. DISCUSSION OF RESULTS

RADIATIVE EQUILIBRIUM

An Example of Radiative Equilibrium.—Figure 12 shows one example of the temperature distribution at radiative equilibrium. The distribution of gases and the solar radiation at 35°N. in April were adopted for this computation. The temperature of the earth's surface was assumed to be 289°K. As a reference, the vertical temperature distribution of the standard atmosphere and that of the dry adiabatic atmosphere are also given in the same figure. According to this figure, the lapse rate of the radiative equilibrium atmosphere is more or less dry-adiabatic up to the 11-km. level except near the ground surface where there is an abrupt decrease of temperature with height. The height of the tropopause is about 11 km. This

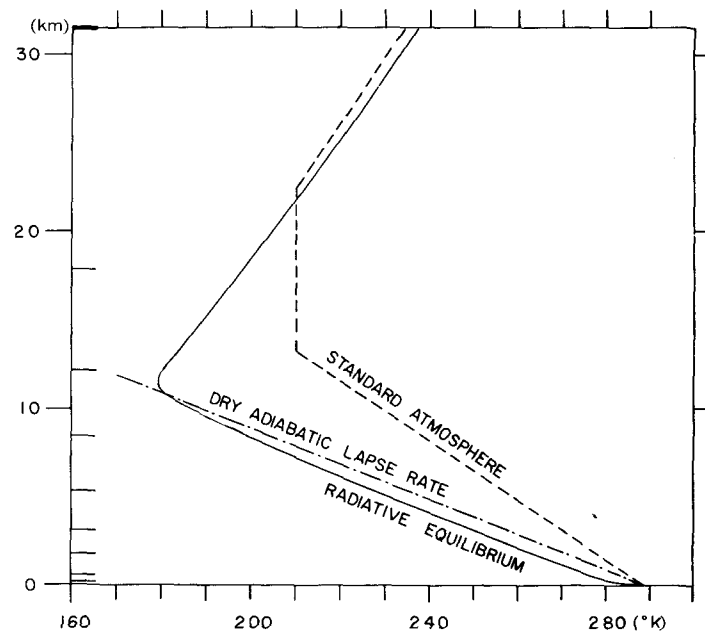


FIGURE 12.—Distribution of radiative equilibrium temperature. The amount of sunshine, the distributions of gases, and surface temperature at 35°N. in April were used ($\delta=0.03^\circ\text{C./day}$). The line of standard atmosphere and that of dry adiabatic lapse rate are also shown for the sake of comparison.

approximately coincides with the observed height of the tropopause in middle latitudes but is much lower than that of the equatorial tropopause. We shall discuss this subject in detail later. The computed tropopause temperature is approximately 180°K. , which is about 20° – 40°K. lower than the observed temperature. Since the frost point of water vapor was assumed to be 190°K. in the lower stratosphere, this computed temperature would cause supersaturation around the tropopause. It is reasonable that the radiative equilibrium temperature of the upper troposphere and lower stratosphere is much lower than the temperature of the standard atmosphere because of the neglect of the process of condensation and that of upward eddy transport of energy from the earth's surface. Above this level the temperature increases sharply with height and again approaches the temperature of the standard atmosphere.

In figure 13 the vertical distribution of various radiative heat balance components corresponding to the quasi-equilibrium temperature of figure 12 is shown. The rapid increase of heating with height due to the absorption of solar ultraviolet radiation by ozone is the main reason for the tendency of temperature increase with height in the stratosphere. This tendency was also obtained by Gowan [22, 23] by taking into consideration the absorption of solar radiation by ozone. If we compare his results with ours, we notice that his radiative equilibrium temperature is much higher than ours. This might be partly due to the fact that he adopted the black-

⁸ The computed equilibrium temperature is warmer than actual.

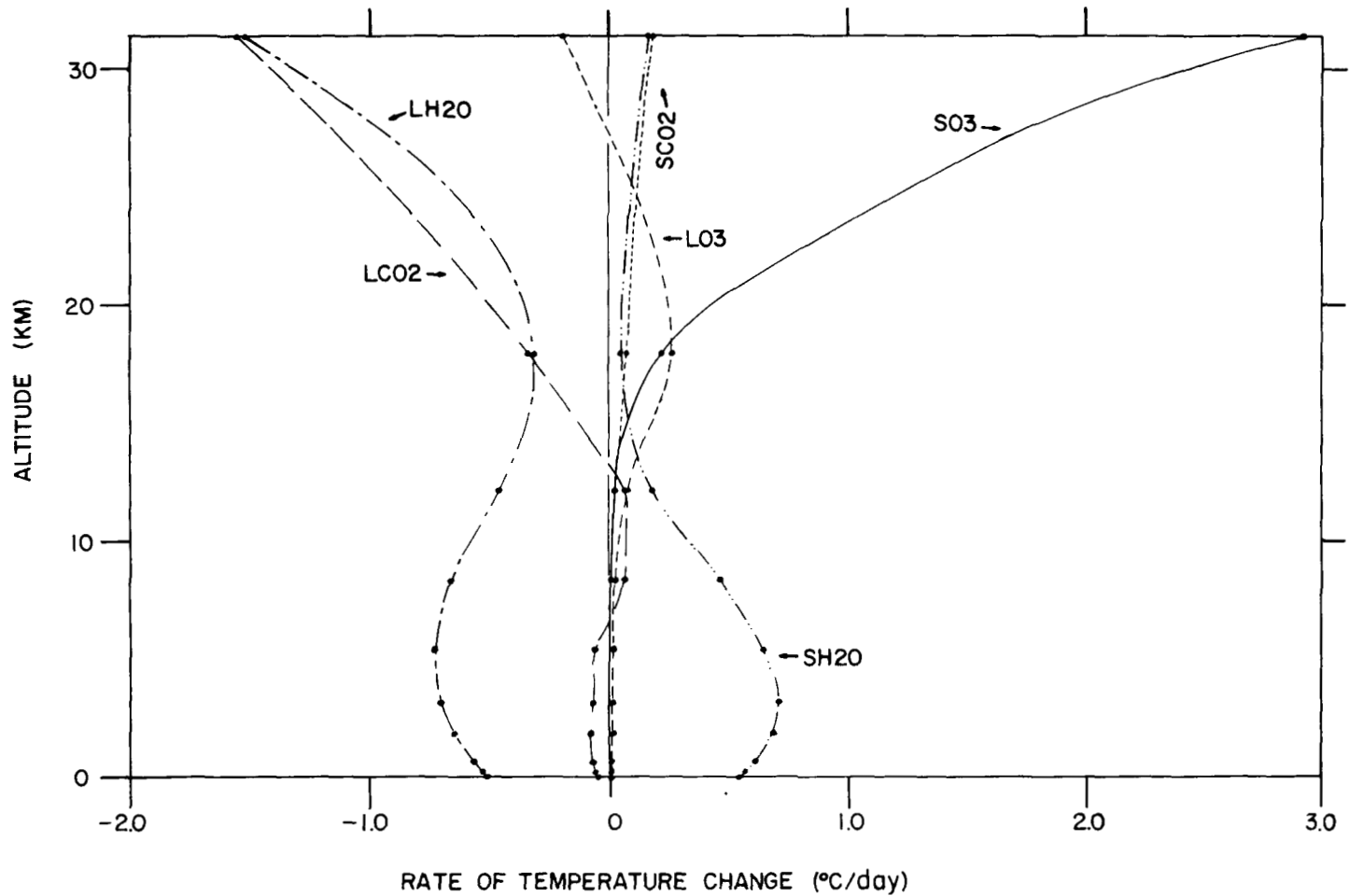


FIGURE 13.—Vertical distribution of the various heat balance components corresponding to the radiative quasi-equilibrium shown in figure 12. SH20, SC02, and SO3 are the rates of temperature change due to the absorption of solar radiation by water vapor, carbon dioxide, and ozone, respectively; and LH20, LCO2, and LO3 are those due to the long wave radiation by water vapor, carbon dioxide, and ozone, respectively.

body radiation at 6000°K . as the solar extraterrestrial radiation. It is now well known that this value of extraterrestrial radiation is much larger than the observed value in the ultraviolet spectrum.

Here we should mention our results obtained by the matrix method, which are to be published in a separate paper [41].⁹ In that paper, instead of assuming the temperature of the earth's surface, we computed it from the condition of radiative equilibrium. The computed temperature of the earth's surface is about 313°K . and is much warmer than the observed value. This is because of the neglect of energy transport from the ground to the atmosphere by turbulent eddies. As a result of this warm surface temperature, the lapse rate of the lower troposphere is somewhat steeper than that of the present computation. However, the height of the tropopause is approximately 11 km. and coincides with the present result. By comparison, Emden's tropopause is located much lower, somewhere around the 6–8-km. level. In the

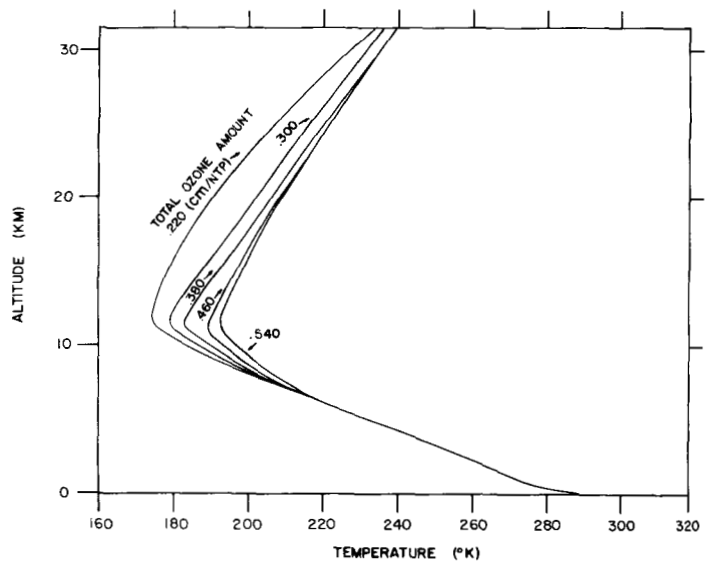


FIGURE 14.—Dependence of equilibrium temperature on the total amount of ozone. The amount of sunshine, distribution of water vapor, and surface temperature at 35°N . in April were used ($\delta = 0.03^{\circ}\text{C./day}$).

⁹ Refer to the end of section 7.

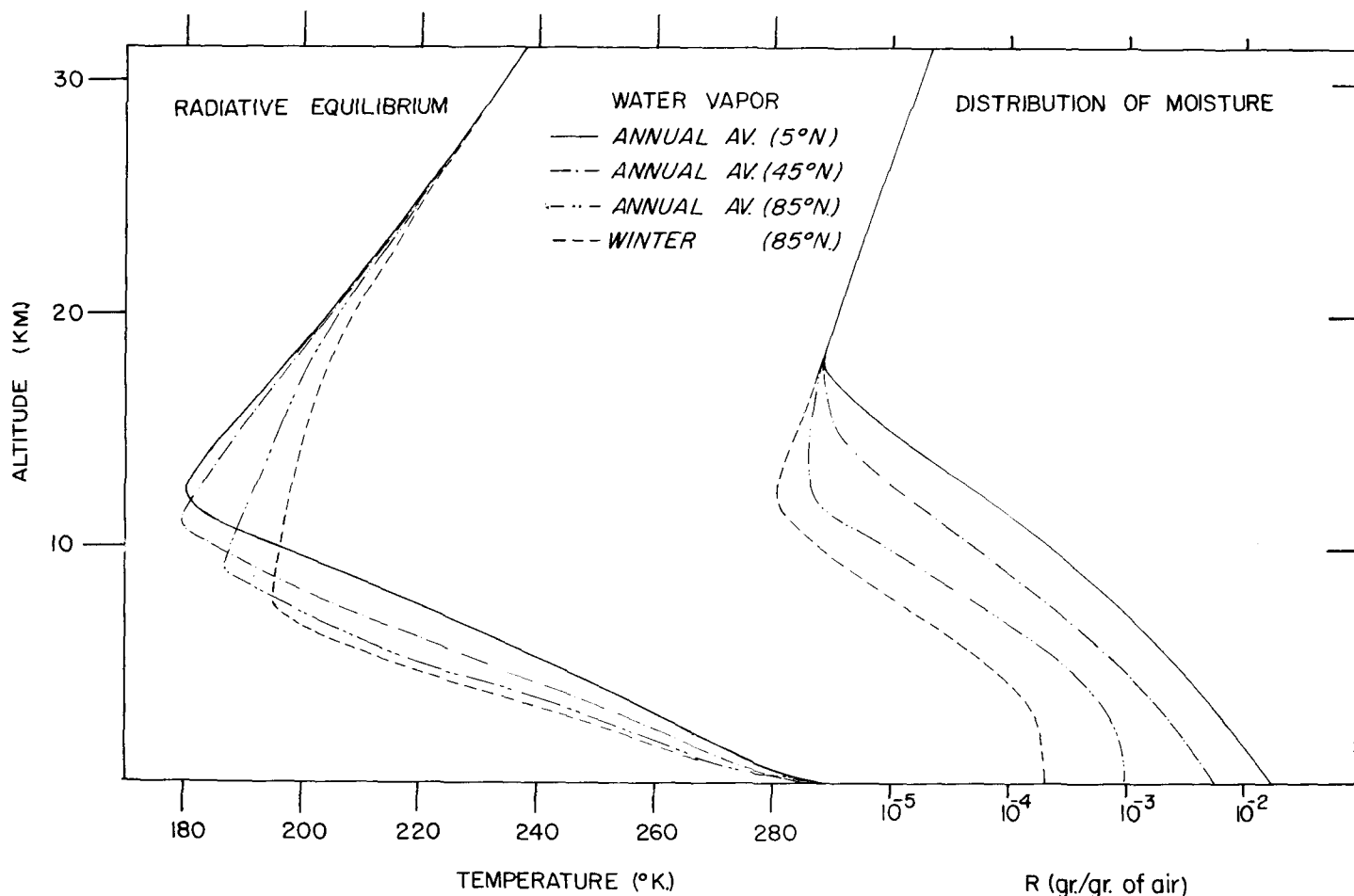


FIGURE 15.—Dependence of equilibrium temperature on the distribution of tropospheric moisture. The distributions of water vapor corresponding to each equilibrium temperature are shown on the right side. The amount of sunshine, distribution of ozone, and surface temperature at 35° N. in April were used ($\delta = 0.03^\circ \text{C./day}$) consistently.

computation by the matrix method, we allowed the possibility of a temperature discontinuity at the earth's surface as was first obtained by Emden [12], whereas in the present computation we did not. The magnitude of temperature discontinuity was very small, about 0.06°C . This is much smaller than the discontinuity of about 20°C . which Emden obtained in his computation of radiative equilibrium based upon the assumption of gray radiation. Accordingly, no large error would be introduced by the neglect of this temperature jump at the earth's surface, which we did in the present computation.

Radiative equilibrium and the distribution of gases.—In order to determine the influence of ozone on the radiative equilibrium, the distributions of radiative equilibrium temperature were computed for various total amounts of ozone, i.e., 0.220, 0.300, 0.380, 0.460, and 0.540 cm./NTP. This range of values includes almost all of the total amounts observed in various latitudes and seasons. The vertical distributions of ozone corresponding to these total amounts are given in figure 11. (Refer to section 6.) The amounts of gases other than ozone and the amount of

sunshine are the average values at 35° N. in April. Figure 14 shows the computed equilibrium temperatures. First of all, we note that the greater the ozone amount, the warmer the radiative equilibrium temperature around the tropopause. The variation of the equilibrium temperature around the tropopause is as much as 20°K . for the range of total ozone amount mentioned above. These results are understandable because, when the total amount of ozone varies, the vertical distribution of ozone varies most markedly around the tropopause (refer to fig. 11). This result suggests that ozone could be one of the important factors causing the increase of stratospheric temperature with latitude. However, as Goody [20] pointed out, the temperature of the earth's surface, which decreases with increasing latitude, is also an important factor in determining the heating due to the 9.6μ band of ozone. This problem will be discussed again by referring to the results of the computation of the heat budget, described in the latter half of this section.

Next, in order to investigate the influence of tropospheric water vapor on the radiative equilibrium tempera-

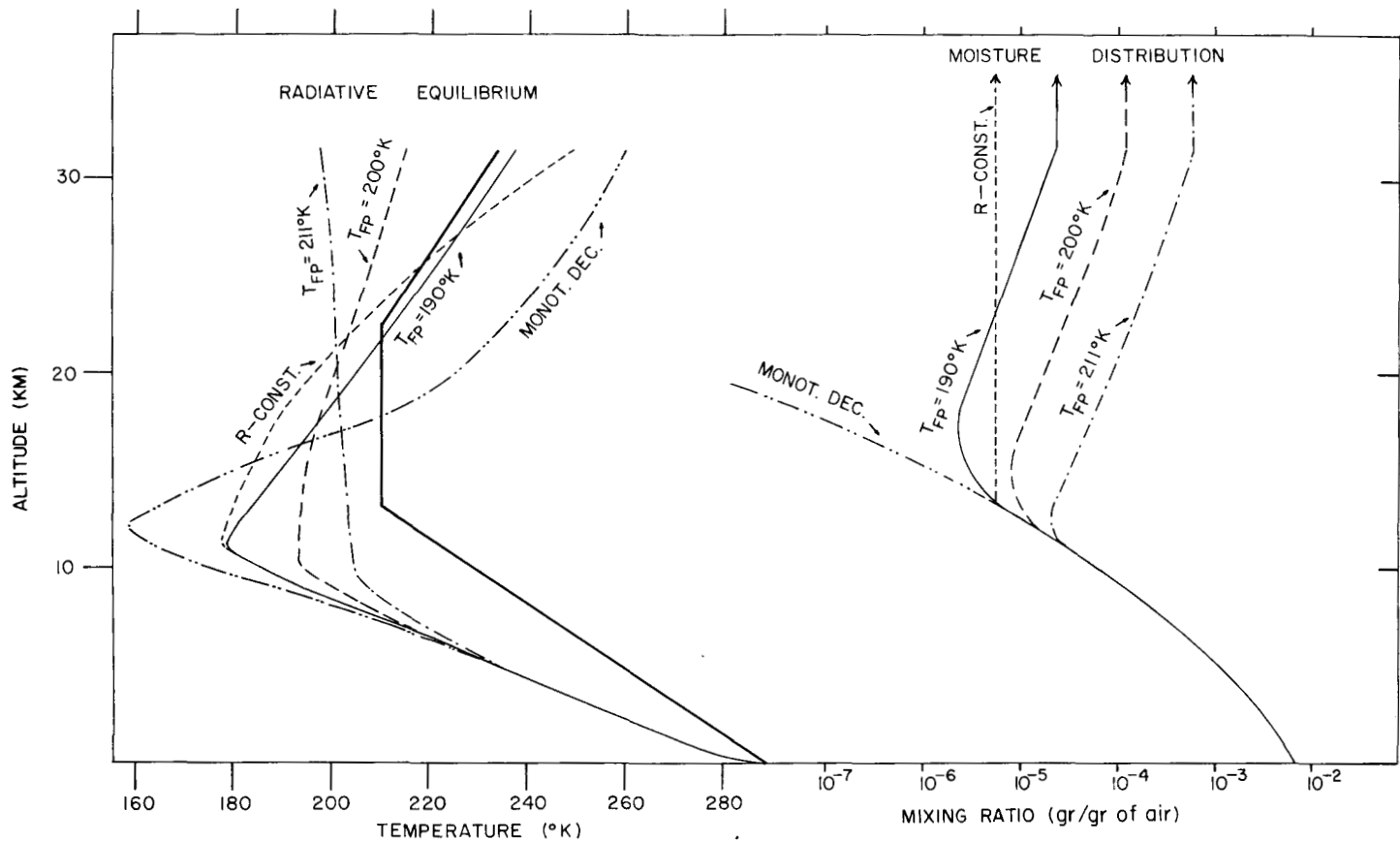


FIGURE 16.—Dependence of equilibrium temperature on the distribution of stratospheric moisture. The distributions of water vapor corresponding to each equilibrium temperature distribution are shown on the right side. The amount of sunshine, distribution of ozone, and surface temperature at 35° N. in April were used ($\delta = 0.03^\circ \text{C./day}$).

ture, equilibrium computations were made for various distributions of tropospheric water vapor. The distributions adopted for these computations are shown on the right hand side of figure 15. They are the annual means of water vapor at 5° N., 45° N., and 85° N., and the distribution at 85° N. in winter. The frost point of water vapor was always assumed to approach the constant value of 190° K. (-83°C.) in the stratosphere. The duration of sunshine, the solar zenith angle, and the distributions of various gases other than water vapor are the mean values at 35° N. in April and are kept the same throughout these computations. The resultant equilibrium temperatures are given on the left hand side of figure 15. The computed height of the tropopause for the low latitude distribution of moisture is higher than that in the high latitudes. The variation of the height of the tropopause over the range of tropospheric water vapor is about 5 km., which is about half of the observed difference in tropopause height between the Pole and the Equator as shown on the left hand side of figure 19. However, these results suggest that the distribution of moisture in the troposphere could be one of the important factors in determining the height of the tropopause. In order to understand these results, it is neces-

sary to examine figure 13. As shown in this figure, the long wave radiation by water vapor is the most important cooling factor near the level of the tropopause. Accordingly, the more water vapor present, the stronger the cooling is. On the other hand, the heating effect due to the absorption of solar radiation by ozone markedly increases with altitude in the stratosphere and that due to the 9.6μ band of ozone also increases with altitude near the tropopause. Since there is usually more water vapor around the tropopause in low latitudes than in high latitudes, the level where the temperature starts increasing with increasing altitude owing to the heating effect of ozone, is higher in low latitudes than in high latitudes.

The importance of the distribution of water vapor as a factor determining the height of tropopause was emphasized by Goody [20] and Yamamoto [70]. Goody explained the latitudinal variation of the height of the tropopause by discussing the balance between the cooling effect of water vapor and the heating effect of the 15μ band of carbon dioxide. We shall discuss this theory in the latter half of this section. Yamamoto computed the temperature distribution of radiative equilibrium for the range of the latitudinal variation of tropospheric moisture

and obtained the correct magnitude of the pole-to-equator difference in the height of the tropopause. His computation, however, is based upon the assumption of gray radiation which gives us much too small absorptivity for the small amount of water vapor existing around the tropopause.

The most uncertain quantity involved in our computations is the distribution of water vapor in the stratosphere, which we discussed in section 6. Therefore, before discussing the computation of latitudinal and seasonal distributions of radiative equilibrium, it seems necessary to know more quantitatively the influence of stratospheric water vapor on the radiative equilibrium temperature profile. On the right hand side of figure 16 the distributions of moisture adopted for this series of computations are given. In order to cover the range of values observed by various authors (refer to fig. 8) we made equilibrium computations for constant frost points of 190°K., 200°K., and 211°K.¹⁰ in the lower stratosphere. Also the radiative equilibrium for a stratosphere with constant mixing ratio¹¹ and one with a monotonical decrease of frost point (6.25°K./km.) were computed. The distributions of tropospheric water vapor and of other gases are the mean values at 35° N. in April.

On the left side of figure 16 the results of the computations are shown, from which we note that the more water vapor which exists in the upper stratosphere, the lower becomes the temperature of the upper stratosphere and the higher the temperature near the tropopause. This is because abundant moisture in the top layer causes strong emission into outer space, and thus the top layer cools more strongly. On the other hand, this moisture increases the downward long wave radiation by water vapor from the top layer, so that the lower layer can be heated more strongly by this radiation. The large difference in the equilibrium temperature of the upper layer of the atmosphere due to the variation of the stratospheric moisture suggests the importance of the continuous and extensive observations of the amount of water vapor. When the amount of water vapor is small, it is difficult to estimate the absorptivity. However, as far as the present results are concerned, the frost point of 190° K., which we are going to adopt consistently in the following computation, seems to give us reasonable temperatures at the highest altitudes involved in our computation.

The series of computations carried out so far suggests that the factor of primary importance in determining the height of tropopause is the distribution of tropospheric moisture. The distribution of ozone and that of water vapor in the stratosphere, however, seem to have an important effect on the temperature around the tropopause. Therefore, indirectly, they could also affect the height of the tropopause by causing a change in the

dynamical behavior of the stratosphere and the upper troposphere.

Seasonal and latitudinal distribution of radiative equilibrium.—Next we shall compute the latitudinal and seasonal variations of equilibrium temperature. The amount of sunshine and the distribution of gases adopted for this computation were described in sections 3 and 6, respectively. Mean observed values for each season and latitude were adopted for the surface temperature, which was assumed to be constant with time. In order to cut the amount of computation, 0.07° C./day was adopted as the convergence criterion δ . This value is slightly larger than the one we have used so far (0.03° C./day). According to our pilot test, the small increase of δ changes the general features of the results very little, if we consistently start from an isothermal atmosphere. (Refer to section 7 for the magnitude of \mathcal{E} corresponding to this δ .)

Figures 17 and 18 give the observed and computed temperature distributions respectively.¹² In spite of the fact that only the effects of radiative processes were taken into consideration, there are various similar features between them. For example, as could be expected from the foregoing study of the effect of tropospheric water vapor, the height of the tropopause is computed to be greater in low latitudes than in high latitudes. In order to compare this computed height with the observed in more detail, we constructed figure 19. On the left hand side of this figure, the seasonal and latitudinal distribution of the tropopause obtained by Kochanski [34] along the 80°W. meridian is given. According to this, the polar tropopause is highest in July, lowest in winter, and higher in October than in spring. In latitudes greater than 60°N., however, the winter tropopause seems to be slightly higher than the spring tropopause. The observed height of the equatorial tropopause in summer is lower than in other seasons, but this tendency does not invariably appear at other longitudes [13]. On the right hand side of this figure the computed heights of the tropopause are shown. The level of minimum temperature, or that of rapid change of lapse rate, was regarded as the tropopause. Since the number of levels where we compute equilibrium temperature is not enough for exact determination of the tropopause, we determined this level by extrapolating the temperature curve from both the tropospheric and stratospheric sides. The difference of the height of the computed tropopause between pole and equator is about 50 percent of that observed. More specifically, the computed height is too low in low latitudes, though it is close to that observed in high latitudes. Qualitatively, the seasonal variation of the height of the tropopause is predicted well, except for the reversal of spring and winter tropopause in high latitude mentioned above. This computed result can be understood by examining the distribution of water vapor around the

¹⁰ $e_{211} \approx 5e_{200} \approx 25e_{190}$ where, for example, e_{200} is the vapor pressure corresponding to the frost point of 200° K. Above the 9-mb. (31.6-km.) level, mixing ratio instead of frost point was assumed to be constant with height.

¹¹ Total amount is the same as the case of 190° K. frost point.

¹² The equilibrium temperature of fall and winter in high latitudes is not shown because the radiative equilibrium is too low to be treated by the present scheme alone.

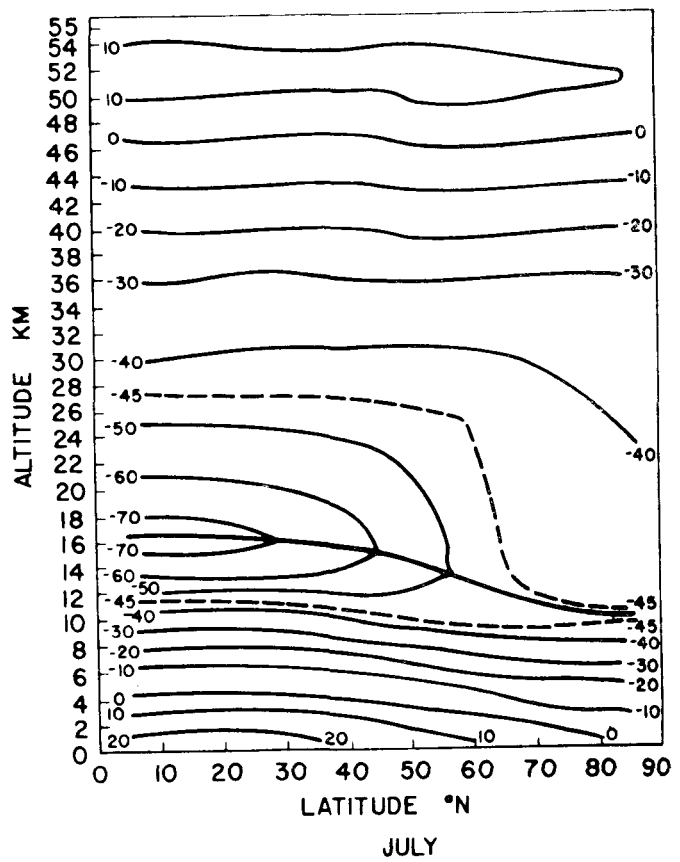
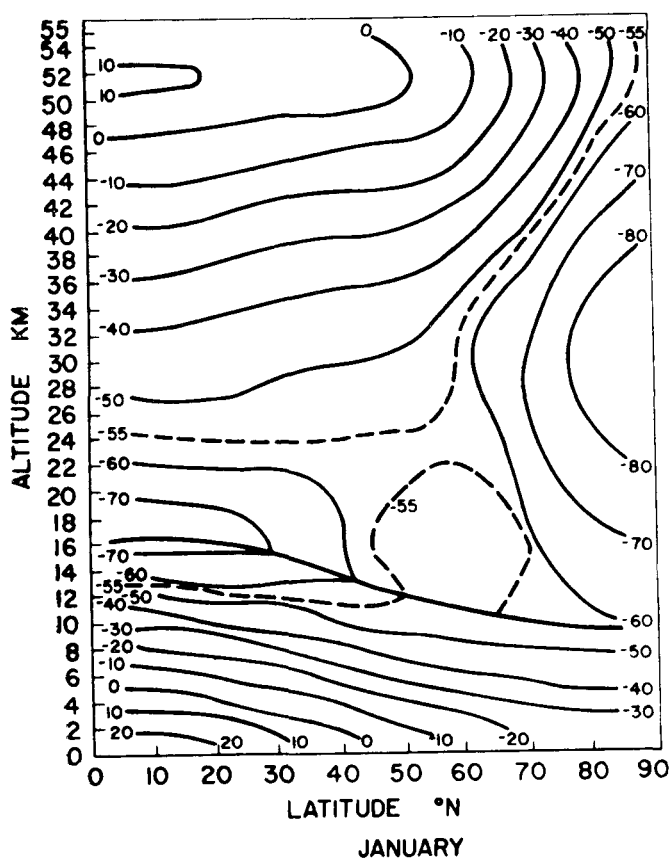
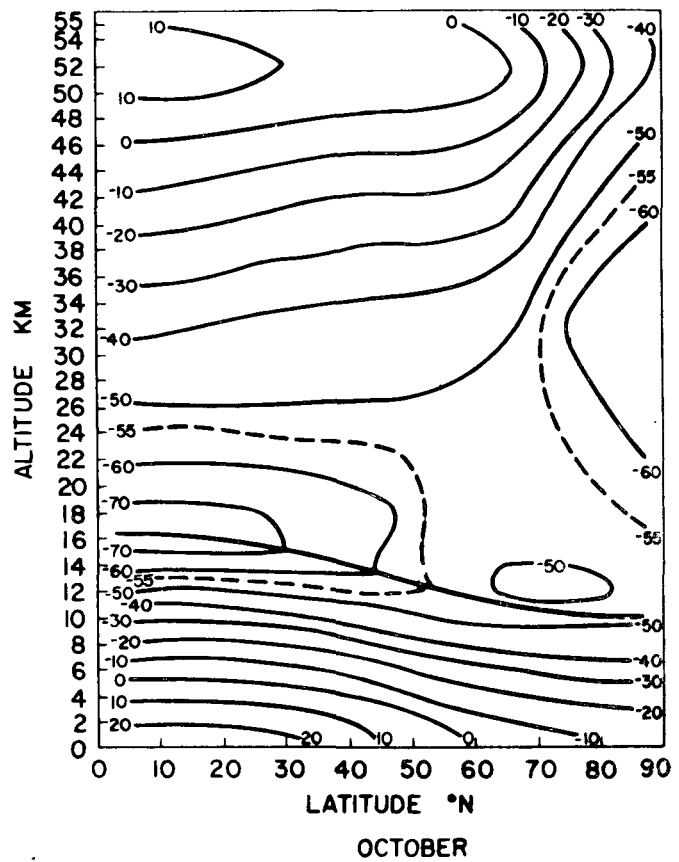
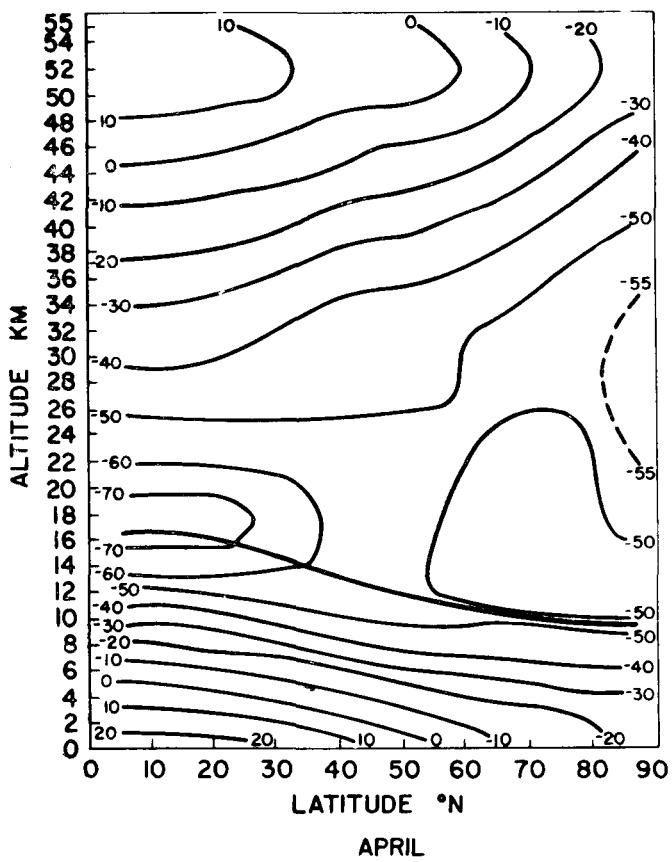


FIGURE 17.—Seasonal and latitudinal distribution of observed temperature compiled by London et al. [35].

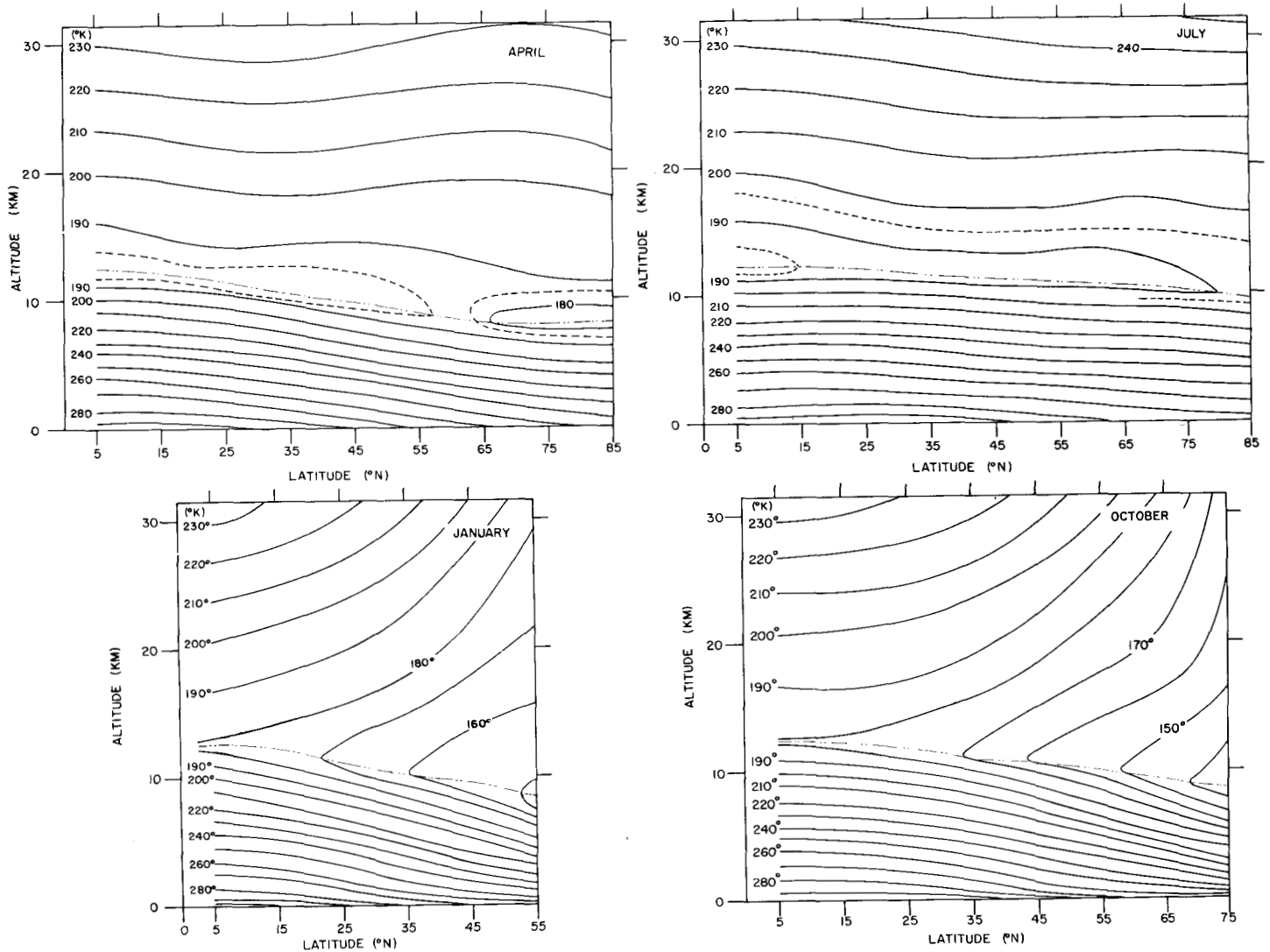


FIGURE 18.—Calculated seasonal and latitudinal distribution of radiative equilibrium. For surface temperature, observed values were adopted ($\delta = 0.07^\circ \text{ C./day}$).

tropopause (refer to fig. 9). Tropopause moisture is maximum in summer, minimum in winter, and greater in autumn than in spring. The failure in predicting the height of the tropopause in low latitudes seems to suggest the importance of the dynamical effect which is not considered in the present computation. It is the next interesting task to find out how the height of tropopause is modified by such phenomena as the meridional circulation in the atmosphere, the cyclone waves, and the moist convection in the lower latitudes.

The observed temperature distributions in figure 17 have a very strong minimum around the equatorial tropopause, irrespective of season, and the temperature of this altitude increases with increasing latitude (except in winter when temperature decreases again in high latitudes). The computed temperature has a slight minimum near the equator and increases very slightly (several degrees) with latitude both in spring and summer.

However, this tendency is much weaker than the observed one. In fall and winter the computed temperature decreases monotonically with latitude.

In order to clarify this conclusion further, we computed the temperature distributions of regional radiative equilibrium at the 74-mb. (18-km.) level, where the equator to pole temperature increase is maximum. As is shown in the Appendix, we use 10 atmospheric temperature levels in our finite difference scheme, and the 74-mb. level is the second level from the top. For other levels observed temperatures were inserted and assumed to remain constant with time. In other words, we computed the temperature of the second level which would maintain the second layer (34–126 mb. or approximately 15–23 km.) in radiative equilibrium if the observed temperatures are given for all other levels. The purpose of this experiment is to find whether or not this layer is in approximate radiative equilibrium with respect to the remainder of the

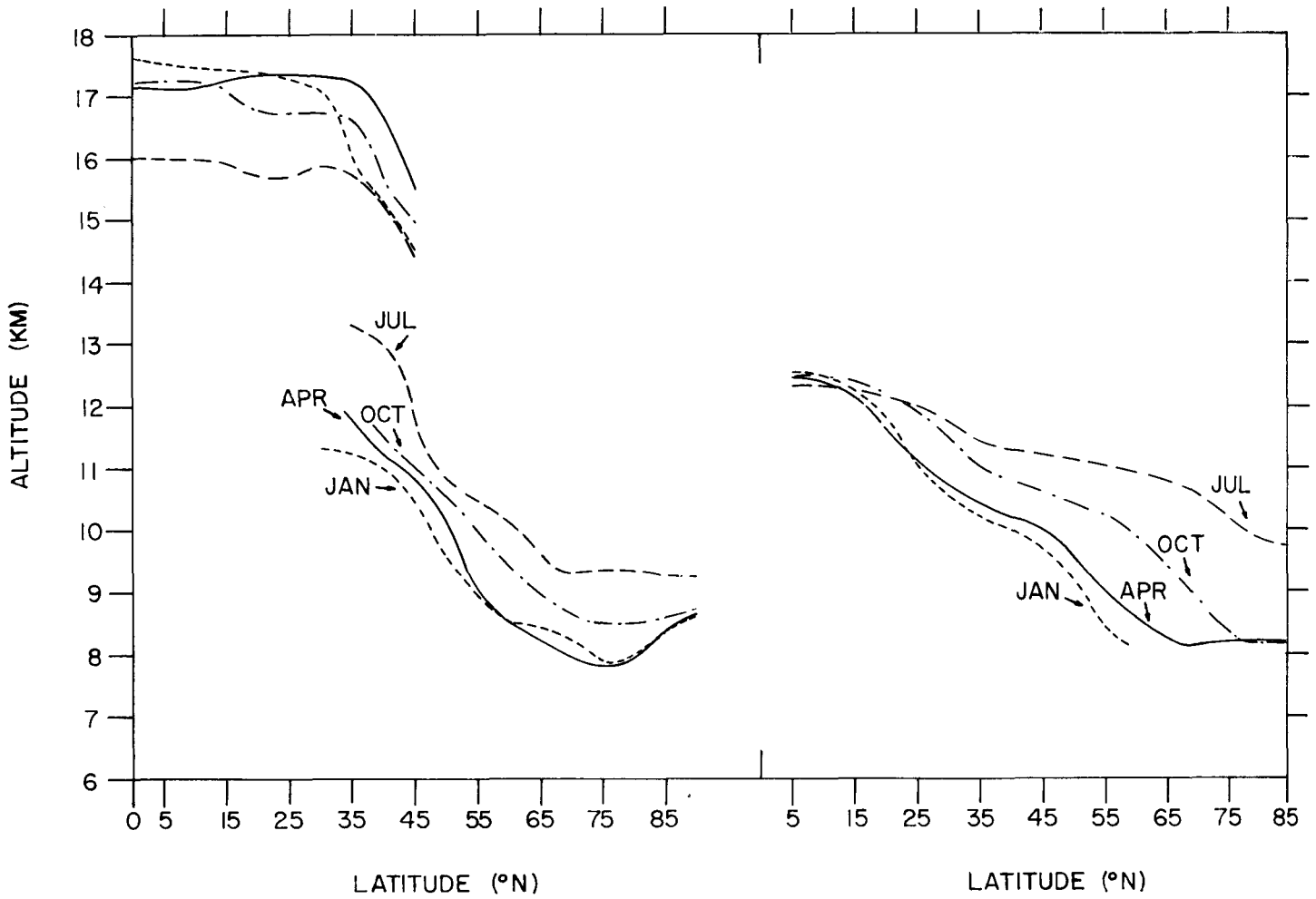


FIGURE 19.—Left side; height of tropopause analyzed by Kochanski [34]. Right side; height of tropopause obtained by equilibrium computation.

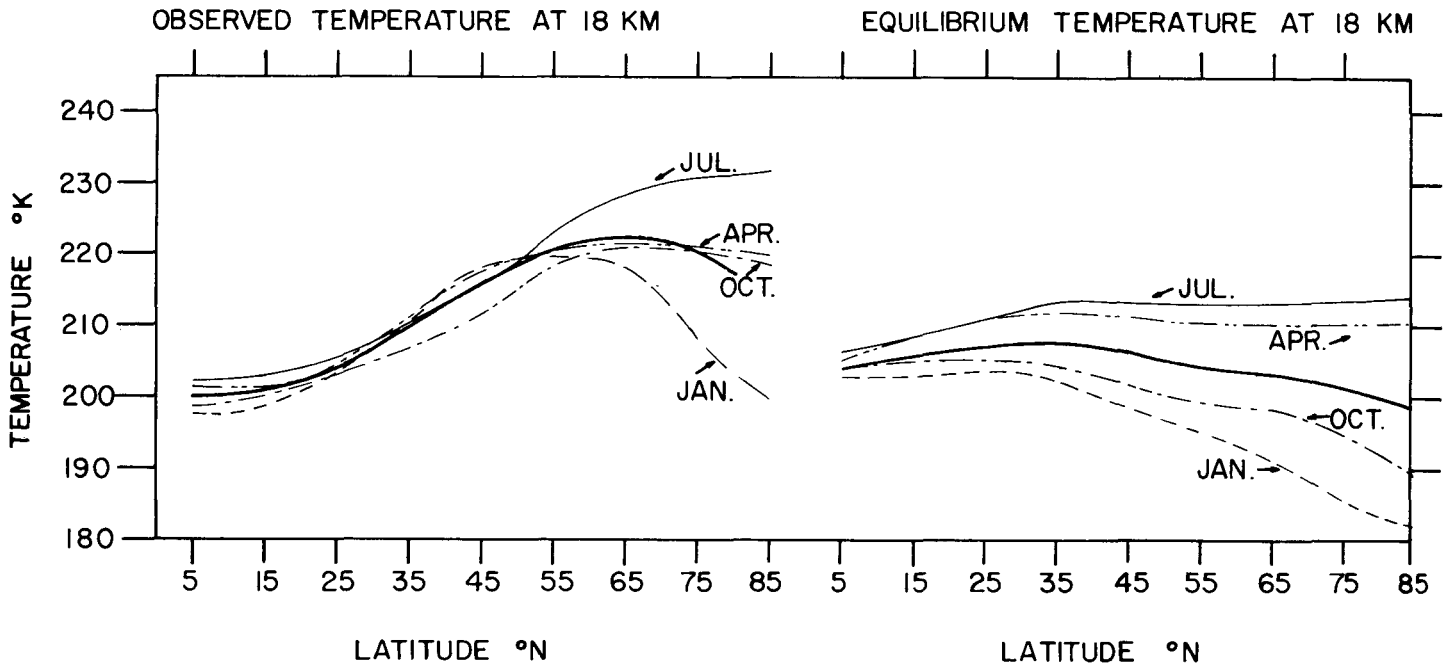


FIGURE 20.—Seasonal and latitudinal distributions of observed (from fig. 17) and computed (right side) temperature of regional radiative equilibrium at the 74-mb. level (18-km. level). As the temperatures of other levels, the observed values were adopted ($\delta = 0.05^\circ \text{C./day}$).

atmosphere, whose temperature we assumed to be that observed. On the left- and right-hand sides of figure 20, observed and computed distributions of temperature at this level are shown. The computed equilibrium temperature reveals some increase with increasing latitude for both summer and spring, but much less than that observed. However the annual averaged equilibrium temperature is more or less isothermal with latitude, whereas the observed mean temperature increases about 17°C . from the equator to the pole. The computed seasonal variations of temperature at this level coincide qualitatively with those observed in higher latitudes, i.e., it is warmest in summer and coldest in winter. In middle latitudes, however, the observed temperature is relatively warm in winter, whereas the computed temperature is coldest. In view of the fact that the degree of baroclinicity is maximum in winter, it would probably be necessary to consider dynamical effects to explain this phenomenon. We shall discuss this problem later.

HEAT BUDGET

The annual mean rate of radiative temperature change.—So far, we have concentrated on a discussion of the computation of radiative equilibrium and have found that the distribution of the radiative equilibrium temperature reveals some of the interesting characteristics observed in the atmosphere. In order to understand these results, however, it is necessary to compute the radiative heat budget of the atmosphere. The distribution of radiative imbalance in the atmosphere would also suggest the effects we should expect on physical processes other than radiative processes. We shall devote the remaining portion of this section to the results of our computation of the radiative heat budget.

The observed distribution of temperature, which was compiled by London et al. [35, 36] and shown in figure 17, was adopted for this computation. The distributions of various atmospheric absorbers were described in section 6. The scheme of computation is similar to that for radiative equilibrium except for the inclusion of the temperature effect on the absorptivity in the calculation of radiative transfer due to the 15μ band of carbon dioxide.

The computed mean annual distribution of the rate of temperature change obtained by taking the average of the heat budget of the four seasons is shown in figure 21. In the stratosphere there is an area of very slight heating in low latitudes and one of cooling in high latitudes. In the troposphere, as is expected, cooling predominates and the area of strong cooling is located in the upper troposphere.

Mean vertical distributions of radiative heat balance components.—In order to determine the relative importance of various radiative processes at each level, hemispheric area mean vertical distributions of temperature changes due to the absorption of solar radiation by water vapor, carbon dioxide, and ozone, and those due to the atmospheric radiation of these gases are shown in figure 22. In the

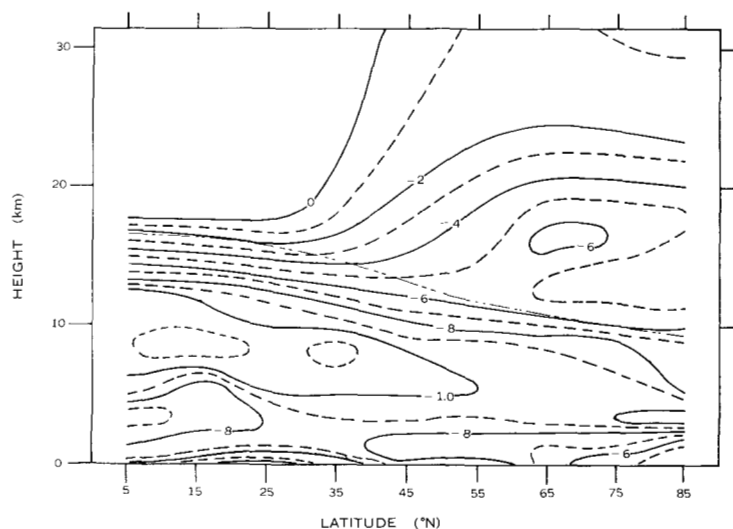


FIGURE 21.—Computed distribution of annual mean rate of temperature change ($^{\circ}\text{C./day}$).

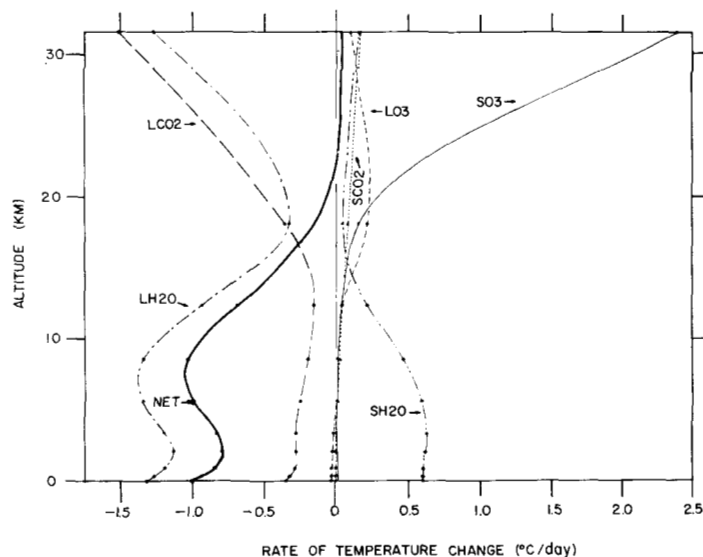


FIGURE 22.—Mean vertical distributions of various heat balance components ($^{\circ}\text{C./day}$). "Net" means the vertical distribution of the net rate of temperature change. For further explanation refer to legend of figure 13.

stratosphere the strong increase of heating with height, due to the absorption of solar radiation by ozone, mainly compensates for that of cooling due to the long wave radiation by both carbon dioxide and water vapor. Owing mainly to the absorption of the radiation coming from the warm ground surface, the radiative transfer of the 9.6μ band of ozone also has a heating effect around the height of 18 km. Relatively speaking, ozone has very important heating effects around this height, where the magnitudes of other radiative processes are rather small.

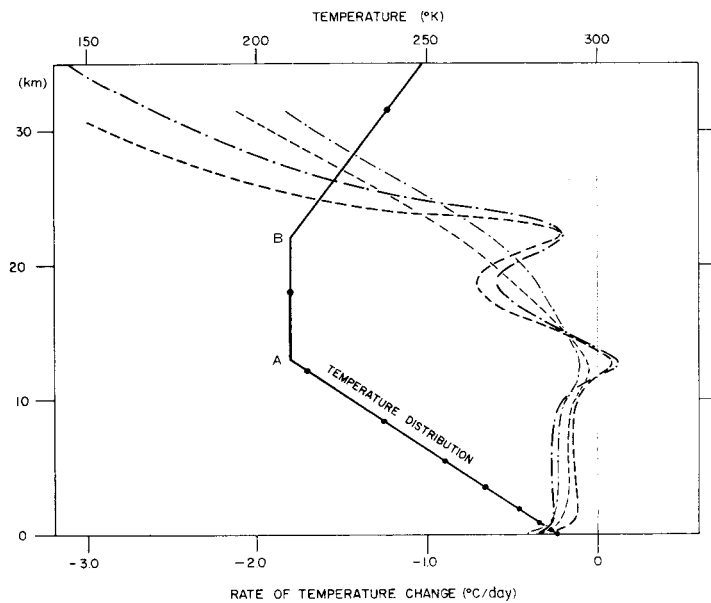


FIGURE 23.—Vertical distribution of temperature change due to the 15μ band of carbon dioxide ($^{\circ}\text{C./day}$). Heavy continuous line is vertical temperature distribution. Plass' [51] results: Heavy dashed line—without temperature effect; heavy dash-dotted line—with temperature effect. Our results: Thin dashed line—without temperature effect; thin dash-dotted line—with temperature effect.

The latitudinal mean effect of the 15μ band of carbon dioxide turned out to be cooling. Because of the weak emission and the absorption of radiation from the warmer regions above and below, this cooling is at a minimum around the tropopause. Above this level it increases with height due to the radiation escaping to outer space. The importance of the 15μ band of carbon dioxide as a cooling effect in the stratosphere has already been emphasized by London et al. [35] and Ohring [48]. However, according to Goody [20], the 15μ band of carbon dioxide has a rather strong heating effect at the tropopause. The reason for this strong heating could be found from a careful examination of Plass' [51] results of the temperature change due to this band. In figure 23 the dash-dotted and dashed heavy lines show the vertical distribution of the rate of temperature change respectively, with and without the temperature effect mentioned before. If we compare these distributions with the vertical distribution of temperature adopted by Plass, we notice that he obtained a sharp maximum heating or minimum cooling at levels A and B where the lapse rate of temperature suddenly changes; i.e., the second derivative of temperature with height has an infinitely large positive value. Therefore, the heating he obtained is a peculiar phenomenon of the tropopause and is not always a characteristic feature of the lower stratosphere. It depends on the magnitude of the discontinuity of lapse rate he assumes for his calculation. This result suggests

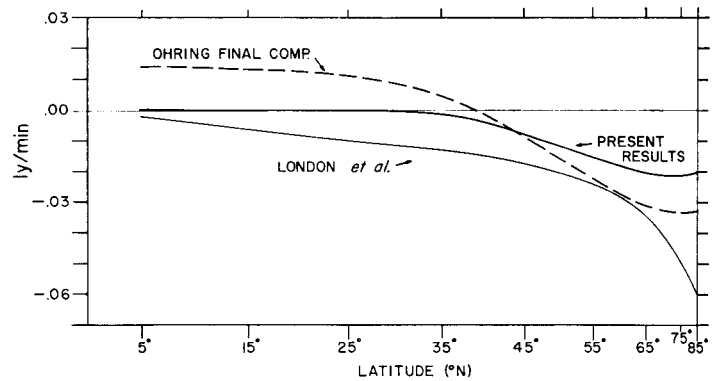


FIGURE 24.—Latitudinal distribution of heat budget in the stratosphere (ly./min.). Heavy solid line—our results. Dashed line—Ohring's [48] final results. Thin solid line—results of London et al. [35].

the necessity for the computation of the latitudinal distribution of heat sources and sinks in the lower stratosphere as well as at the tropopause which Goody [20] computed. For comparison, the results which are obtained from our scheme are also included in the same figure. Since our computations were made for fewer levels than those of Plass [51], his results include many more detailed features. The overall features of stratospheric cooling do not, however, differ from each other. The cooling obtained by including the temperature effect on CO_2 is smaller in the stratosphere and is larger in the troposphere than that obtained by neglecting it. The heating due to the absorption of solar radiation by carbon dioxide is very small compared with the effects of other processes. However around the tropopause, where the contributions of various radiative processes are at a minimum, it is not always negligible.

The cooling due to the long wave radiation by water vapor is maximum in the upper troposphere owing to the sharp decrease of water vapor with height. This constitutes the emission layer mentioned before. The heating due to the absorption of solar radiation by water vapor is mainly important in the troposphere and is very small in the stratosphere as compared with the magnitude of other effects.

Summing all these contributions, the net rate of temperature change due to all of these radiative processes is also shown in figure 22. Owing to the sharp increase of heating by ozone with increasing altitude, this net rate has the effect of intensifying the existing stratospheric inversion. This result is consistent with the typical inversion which appeared in the stratosphere of our radiative equilibrium. The degree of radiative imbalance is largest in the upper troposphere and becomes smaller as we go higher into the stratosphere. This result seems to be reasonable because one may expect more transfer of tropospheric energy into the lower stratosphere than to the upper stratosphere. However it must also be kept in mind

that the higher the altitude, the less accurate is our scheme of computation and the assumed distributions of the absorbing gases. Therefore in order to verify these results it is necessary to make more careful observations of the distributions of gases and to have more exhaustive laboratory experiments to determine the absorptivity of these gases.

Latitudinal distributions of radiative heat balance components.—Next, we shall discuss the latitudinal distribution of heat sources and sinks in the stratosphere. In figure 24 the results of our computation of the stratospheric heat budget are shown together with that of London et al. [35] and the revised result by Ohring [48]. The heights of the tropopause used for this computation are the same as those compiled by London [36]. The difference among these results might be considered to be a manifestation of the degree of ambiguity involved in this type of computation. The one common feature is, however, the increase of the tendency of cooling with increasing latitude.

In order to find out how the various radiative processes combine to make up this latitudinal distribution of stratospheric heat budget, we examined the contribution of each process at the 74-mb. (18-km.) level,¹³ where the temperature increases most sharply with increasing latitude. In figure 25 are shown the latitudinal variations of the annual average of the rate of temperature changes due to the radiative processes. At this level the heating factors are the long wave radiation of ozone and the absorption of the solar radiation by ozone, carbon dioxide, and water vapor; the cooling factors are the long wave radiation by carbon dioxide and water vapor.

As we could expect, the heating due to the absorption of solar radiation by water vapor and carbon dioxide decreases with increasing latitude; that by ozone, however, hardly decreases at all owing to the sharp latitudinal increase of ozone at this level and the increase of the zenith angle of the sun.

The cooling due to the long wave radiation of water vapor is more or less constant with latitude in spite of the fact that the troposphere is cooler with increasing latitude. This is partly due to the slight latitudinal decrease of water vapor contained in this layer (34–126 mb. or approximately 23–15 km; refer to Appendix I). Another important reason is the lowering with increasing latitude of the height of the effective source of tropospheric emission which reaches the lower stratosphere. As was pointed out by Simpson [56] the more water vapor that exists in the atmosphere, the lower is the temperature of the effective source of long wave radiation leaving the atmosphere, because when water vapor is abundant, the radiation which is emitted from the lower atmosphere is absorbed again by the water vapor existing in higher altitudes.

¹³ Since the rates of the temperature change at this level were obtained by subtracting the net flux at the 126-mb. (15-km.) level from that at the 34-mb. (23-km.) level, it might be more reasonable to regard them as the average rates of this whole layer.

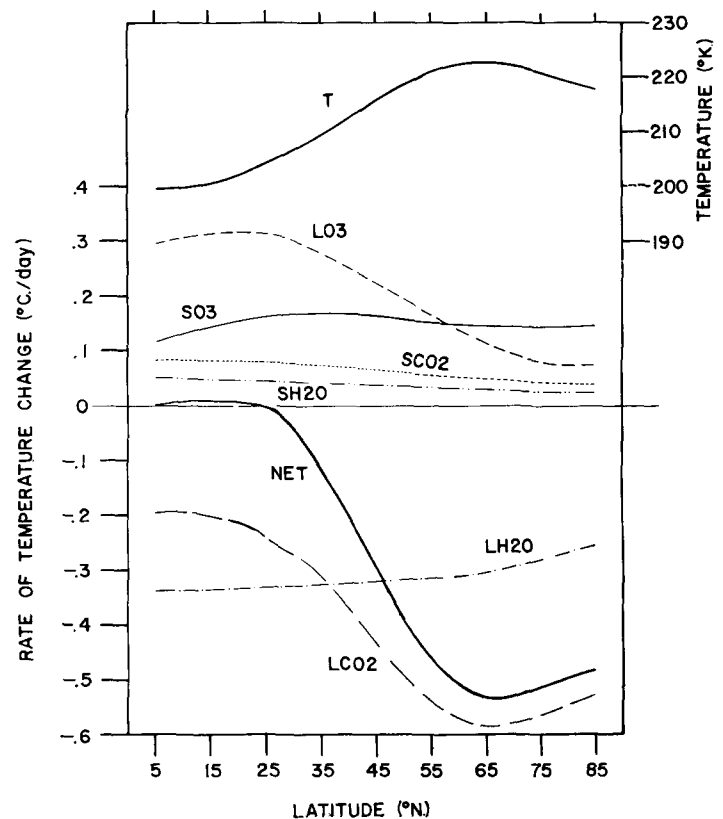


FIGURE 25.—Latitudinal distribution of annual mean rate of temperature change due to various radiative processes at 74-mb. level (18-km. level). *T* denotes the annual mean temperature in degrees Kelvin. For further explanation refer to legend of figure 13.

The heating due to the 9.6μ band of ozone increases with latitude up to about 30° N. due to the latitudinal increase of ozone, but it decreases again in higher latitudes because of the decrease of the temperature of the earth's surface with latitude. This result coincides with Goody's [20] conclusion that the latitudinal variation of heating due to the 9.6μ band of ozone could hardly be a factor to explain the latitudinal increase of temperature in the lower stratosphere because the effect of the sharp increase of the ozone amount with increasing latitude at this 18-km. level is countered by that of the decrease of the earth's surface temperature with increasing latitude.

The cooling due to the 15μ band of carbon dioxide sharply increases with increasing latitude because of both the latitudinal increase of temperature at this level and the latitudinal decrease of the temperature of the troposphere. A recent computation by Brooks [7] shows the same tendency, although the magnitude of the rate of the cooling he obtained is slightly larger than ours¹⁴ (by

¹⁴ This discrepancy might be due partly to his neglect of the temperature effect on absorption of carbon dioxide. In order to compare his results with ours, we integrated his results to obtain the average rate of temperature change between the 34-mb. and 126-mb. levels

about 0.2°C./day). This tendency explains why we could not simulate sufficiently the increase of temperature in the stratosphere with increasing latitude by our computation of radiative equilibrium despite the favorable effect of water vapor.

The latitudinal increase of the cooling of the layer around the 18-km. level due to the 15μ band of carbon dioxide and the cooling in the lower stratosphere of high latitude due to the long wave radiation of water vapor are the main causes of the net cooling in the stratosphere of the higher latitude which appears in figures 21 and 24. It is possible to speculate on various processes which have been suggested by various authors and which could compensate for this cooling tendency of the stratosphere in higher latitudes, e.g.:

(1) Northward transport of heat by large-scale eddies at the 100-mb. level against the temperature gradient. This was suggested by Starr and White [58] based upon their statistical analysis of radiosonde data. The moist convection at low latitudes, which penetrates into the high troposphere, could supply heat in compensation for the heat sink caused by northward transport.

(2) A meridional circulation in the stratosphere directed downward in high latitudes. This possibility was suggested by Brewer [6].

(3) Upward transfer of heat energy by large-scale disturbances of higher latitude accompanied by the release of potential energy into kinetic energy.

In order to determine the process or processes of major importance, it would be desirable to perform a careful investigation of the distributions of radioactive debris introduced into the high atmosphere by atomic explosions and those of rare gases as well as to conduct numerical experiments by use of advanced general circulation models which include both the hydrodynamical behavior of the atmosphere and radiative transfer.

9. CONCLUSIONS

(1) The vertical distribution of radiative equilibrium temperature was obtained as the balance among various radiative processes, i.e., the absorption of solar radiation by water vapor, carbon dioxide, and ozone, and the long wave radiation by these three gases. For the surface temperature, the observed value was adopted. Below the level of 11 km., we get a nearly dry adiabatic lapse rate except near the ground where there is a superadiabatic layer. Above 11 km. there appears a radiative equilibrium stratosphere, where temperature increases slowly with altitude, mainly because of the increase of the absorption of solar radiation by ozone. The computed temperature near the tropopause is much cooler than observed (by 20° – 40°C.) as a result of the neglect of other processes such as dry and moist convection and vertical transfer of heat by the large-scale eddies.

(2) The latitudinal and seasonal distributions of the computed tropopause heights compare fairly well with those of the observed polar tropopause. They are highest in low latitude and lowest in high latitude; they are highest in summer, lowest in winter, and higher in fall than in spring. However, the tropopause in low latitudes is considerably lower than the observed equatorial tropopause. The pole to equator difference of height of the computed tropopause is about 50 percent smaller than that observed.

(3) The distribution of the computed height of the tropopause has a close correspondence with that of water vapor in the upper troposphere. Generally speaking, when more water vapor exists around the tropopause, the computed height of the tropopause is higher and its temperature is lower.

(4) The computed temperature of radiative equilibrium at the 18-km. level increases slightly (about 7°C.) from equator to pole both in summer and spring, but decreases monotonically in winter and fall. The actually observed annual mean temperature increases about 20°C. from equator to pole at this level. This tendency is maximum in summer.

(5) The large range of computational results of the radiative equilibrium temperature for the observed range of stratospheric moisture suggests a strong necessity for further accurate water vapor measurements in the stratosphere.

(6) According to our computation of radiative heat budget, in the stratosphere, net heating effects include the absorption of solar radiation by water vapor, carbon dioxide (not negligible around the tropopause), and ozone and the atmospheric radiation due to the 9.6μ band of ozone; net cooling effects include the long wave radiation by water vapor and carbon dioxide. Summing all these contributions we obtain a very weak heating in low latitudes and a rather strong cooling in the lower stratosphere at high latitudes. This cooling is too large to be considered as the product of uncertainties involved in the computation and must be compensated for by heat transfer processes other than radiation.

(7) In order to verify conclusion (4), the study of various processes contributing to the heat budget of the layer around the 18-km. level, where the observed temperature most sharply increases with latitude, was performed. The long wave radiation by water vapor has a tendency to maintain the existing latitudinal gradient. The effects of ozone have the same tendency in low latitudes but not in high latitudes. The long wave radiation by carbon dioxide has a strong tendency to destroy the existing latitudinal increase of temperature. The net effect of these radiative processes could barely maintain the stratospheric temperature approximately constant with latitude and hardly explains the sharp latitudinal temperature increase observed in the stratosphere.

10. CRITICAL COMMENTS AND FUTURE WORK

In order to obtain simply the radiative equilibrium of the atmosphere, we have made various assumptions. They should, however, be removed for the more detailed discussion of the phenomenon. One of the most important assumptions is the neglect of the effect of clouds. Therefore, a method of incorporating the effect of clouds has been worked out and is being programmed for the high speed computer. The influence of clouds on the radiative equilibrium and the earth's climate is one of the major items which we should investigate before we incorporate the radiative processes into the general circulation models.

Since we completed the writing of this paper, new studies on the absorptivities and distributions of atmospheric gases have been published. These new data will be considered in a forthcoming study.

ACKNOWLEDGMENTS

The authors wish to express their hearty thanks to Dr. J. Smagorinsky who originally suggested that this work be done and has given us very helpful suggestions and constant encouragement throughout this work; and to Drs. D. K. Lilly, G. Yamamoto, D. Q. Wark, and S. Fritz who have always given us many valuable suggestions. They are also indebted to Mr. R. Strickler who carefully checked the computation scheme and improved the coding, to Mr. E. Riesenbergl who did the programming throughout our study, and to Mr. E. Rayfield and Mrs. J. Snyder who assisted with the preparation of the figures and manuscript, respectively.

APPENDIX I

VERTICAL COORDINATE SYSTEM

In order to perform the numerical computation of the radiative change of temperature, it is first of all necessary to specify the levels where we carry the values of temperature. Needless to say, the more levels we have the smaller the truncation errors due to differencing. However, it is wise to adopt the minimum number of levels consistent with the small truncation error required, because an increase in the number of levels is accompanied by a large increase in the amount of computation.

The coordinate system used in our computation is the one proposed by Smagorinsky for an advanced model to study the general circulation of the atmosphere. This system is designed in such a way as to give us a higher resolution in the surface boundary layer and in the stratosphere where temperature varies remarkably with respect to pressure. Therefore, this coordinate system is very convenient in minimizing the number of layers which are necessary to express the vertical structure of the atmosphere. According to the proposal of Smagorinsky, his σ -coordinate system is connected with the p -coordinate system by the following equation.

$$p/p_* = \sigma^2(3 - 2\sigma) \tag{A-1}$$

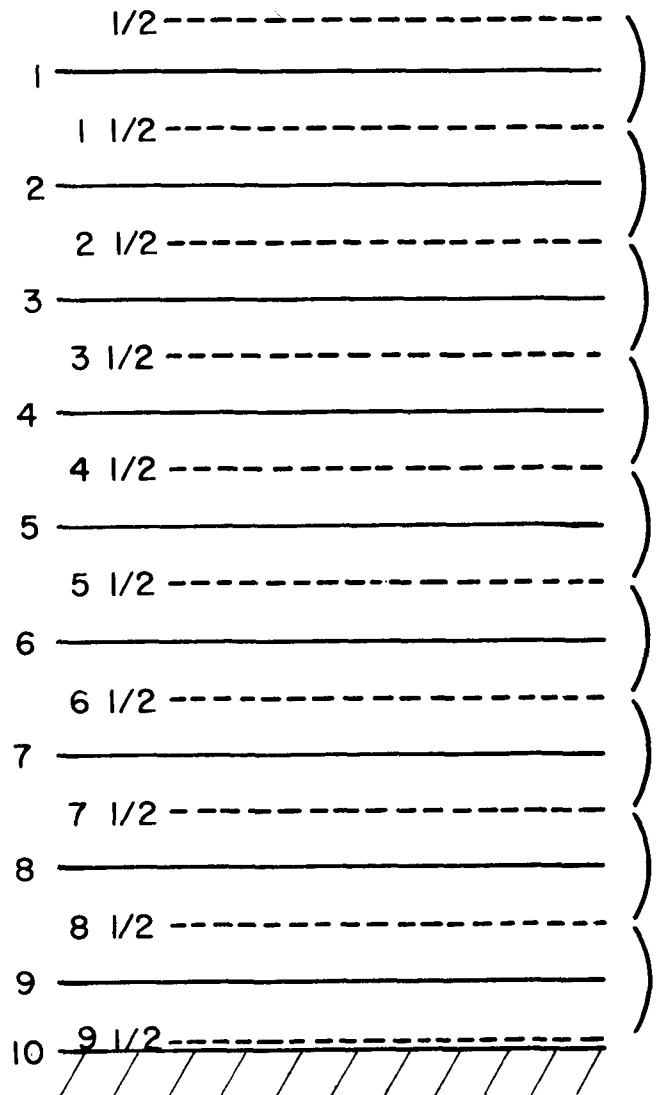


FIGURE 26.—Indexing of layers. $I=1/2$: top of atmosphere, $I=9 1/2$: bottom of atmosphere. $I=10$: earth's surface (same height with level $9 1/2$).

where p_* is the pressure at the earth's surface. Throughout our computation this p_* is assumed to be 1000 mb. Using this system, we divided the atmosphere into nine layers; i.e., into nine equal σ -intervals, which are shown in figure 26. Also, in table 5 the height and pressure of each level and the pressure thickness of each layer are shown. The boundaries between two neighboring layers are described by half integers. Temperature is specified at each integer level. Near the ground surface, the height of the level changes approximately logarithmically so that temperature could vary approximately linearly from one level to another. In the formulation of finite difference equations (Appendix III) it is assumed that temperature could be linearly interpolated with respect to this σ -coordinate system.

TABLE 5.—Illustration of σ -coordinate system and the list of input specified for each σ -level. Δp is pressure thickness of each layer, H is height of each level. (ICAO standard atmosphere; adjustment was made such that the height of 1000 mb. is zero)

I	σ	p (mb.)	Δp (mb.)	H (km.)
$\frac{1}{2}$	0.0000	0	—	∞
1	0.0555	9	34	31.6
$1\frac{1}{2}$.1111	34	—	23.0
2	.1666	74	92	18.0
$2\frac{1}{2}$.2222	126	—	14.7
3	.2777	189	133	12.0
$3\frac{1}{2}$.3333	259	—	10.1
4	.3888	336	158	8.3
$4\frac{1}{2}$.4444	417	—	6.8
5	.4999	500	166	5.5
$5\frac{1}{2}$.5555	583	—	4.3
6	.6110	664	158	3.3
$6\frac{1}{2}$.6667	741	—	2.5
7	.7221	811	133	1.7
$7\frac{1}{2}$.7778	874	—	1.1
8	.8332	926	92	.64
$8\frac{1}{2}$.8889	966	—	.3
9	.9443	991	34	.07
$9\frac{1}{2}$	1.0000	1000	—	.00
10	1.0000	1000	—	.00

APPENDIX II

EMISSIVITIES AND ABSORPTIVITIES

The values of ϵ_f^w , ϵ_f^o , \mathcal{E}_f^G ($G=C$ or O), and a^G ($G=W$, C , or O) are tabulated for every increment of 0.5 of the logarithm of effective optical thickness. Using this table, the values of absorptivities were determined for any value of optical thickness by linear interpolation with respect to the logarithm of effective optical thickness.

In the upper troposphere the mixing ratio of water vapor changes approximately exponentially with height. Therefore, when we computed the optical thickness of water vapor, the exponential variation of water vapor was assumed between the neighboring integer levels where the mixing ratio was specified.

APPENDIX III

FORMULATION OF THE FINITE DIFFERENCE EQUATION

In order to show how we changed the equations for the temperature change due to atmospheric radiation into the finite difference equation, we shall transform the second term of equation (17) into finite difference form as an example. If we consider the case when the index of the height z is $I+\frac{1}{2}$ the second term should be written as

$$\int_{b_{I+\frac{1}{2}}^G}^{b_I^G} \mathcal{E}_f(y) \pi db^G = \int_{b_{I+\frac{1}{2}}^G}^{b_I^G} \mathcal{E}_f^G(y) \pi db^G + \sum_{K=1}^{I-1} (b_K^G - b_{K+1}^G) \cdot \mathcal{E}_f^G(K+\frac{1}{2}, I+\frac{1}{2}) + \int_{b_{I+\frac{1}{2}}^G}^{b_I^G} \mathcal{E}_f^G(y) \pi db^G \quad (\text{A-2})$$

where, for example, $\mathcal{E}_f^G(K+\frac{1}{2}, I+\frac{1}{2})$ is the band absorptivity of the layer of optical thickness $u_r(K+\frac{1}{2}, I+\frac{1}{2})$ ($\equiv [(u_r)_{K+1/2} - (u_r)_{I+1/2}]$), and b_K^G is the abbreviation of b^G for temperature T_K .

Since we do not know the temperature at the top of the atmosphere ($T_{\frac{1}{2}}$) we made the following assumption

for the sake of simplicity (refer to equation (41)),

$$T_{\frac{1}{2}} = T_1 \quad (\text{A-3})$$

and adopted the following approximation:

$$\int_{b_{I+\frac{1}{2}}^G}^{b_I^G} \mathcal{E}_f^G(y) \pi db^G \approx (b_I^G - b_{I+\frac{1}{2}}^G) \cdot \left\{ (1/u_r(I, I+\frac{1}{2})) \int_0^{u_r(I, I+\frac{1}{2})} \mathcal{E}_f^G(u_r) du_r \right\} \quad (\text{A-4})$$

The integral (A-2) is to be approximated as follows:

$$\int_{b_{I+\frac{1}{2}}^G}^{b_I^G} \mathcal{E}_f^G(y) \pi db^G \approx \sum_{K=1}^{I-1} (b_K^G - b_{K+1}^G) \cdot \mathcal{E}_f^G(K+\frac{1}{2}, I+\frac{1}{2}) + (b_I^G - b_{I+\frac{1}{2}}^G) \left\{ (1/u_r(I, I+\frac{1}{2})) \int_0^{u_r(I, I+\frac{1}{2})} \mathcal{E}_f^G(u_r) du_r \right\} \quad (\text{A-5})$$

The quantity in the second bracket of the third term was computed by interpolating the table. The reason we adopted this special treatment is the highly non-linear change of \mathcal{E}_f^G with respect to u_r when u_r tends to zero. Based upon equation (1), the temperature change at integer levels due to the long wave radiation of water vapor is to be expressed by the following finite difference form:

$$\left(\frac{\partial T_K}{\partial t} \right)_{LR}^w = \frac{g}{c_p} \frac{1}{p_{K+\frac{1}{2}} - p_{K-\frac{1}{2}}} [F_{K+\frac{1}{2}}^w - F_{K-\frac{1}{2}}^w] \quad (\text{A-6})$$

($K=1, 2, \dots, 9$)

The finite difference equation for the rate of temperature change due to the absorption of solar radiation will not be described here, because it can be derived from equation (27) without difficulty.

REFERENCES

1. A. Adel and C. O. Lampland, "Atmospheric Absorption of Infrared Solar Radiation at the Lowell Observatory; 5.5 $\sim 14\mu$," *Astrophysical Journal*, vol. 91, 1940, pp. 481-487.
2. F. R. Barclay, M. J. W. Elliott, P. Goldsmith, and J. V. Jellay, "A Direct Measurement of the Humidity in the Stratosphere Using a Cooled-Vapor Trap," *Quarterly Journal of the Royal Meteorological Society*, vol. 86, No. 368, Apr. 1960, pp. 259-264.
3. E. W. Barrett, L. R. Herndon, Jr., and H. J. Carter, "Some Measurements of the Distribution of Water Vapor in the Stratosphere," *Tellus*, vol. 2, No. 4, Nov. 1950, pp. 302-311.
4. W. S. Benedict, "Theoretical Studies of Infrared Spectra of Atmospheric Gases," *Final Report on Contract AF19(604)-1001*, Laboratory of Astrophysics and Physical Meteorology, Johns Hopkins University, June 1956, 66 pp.
5. D. Brunt, *Physical and Dynamical Meteorology*, 2d Ed., Cambridge University Press, Cambridge, 1941, (pp. 129-134).
6. A. W. Brewer, "Evidence for a World Circulation Provided by the Measurements of Helium and Water Vapour Distribution in the Stratosphere," *Quarterly Journal of the Royal Meteorological Society*, vol. 75, No. 326, Oct. 1949, pp. 351-363.
7. D. L. Brooks, "The Distribution of Carbon Dioxide Cooling in the Lower Stratosphere," *Journal of Meteorology*, vol. 15, No. 2, Apr. 1958, pp. 210-219.

8. R. A. Craig, "The Observations and Photochemistry of Atmospheric Ozone and Their Meteorological Significance," *Meteorological Monographs*, American Meteorological Society, vol. 1, No. 2, 1950, 50 pp.
9. H. A. Daw, "Transmission of Radiation Through Water Vapor Subject to Pressure Broadening in the Region 4.2 microns to 23 microns," *Technical Report No. 10*, Contract AF19(122)-392, University of Utah, 1956.
10. G. M. B. Dobson, A. W. Brewer, and B. M. Cwilong, "Meteorology of the Lower Stratosphere," *Proceedings of the Royal Society of London*, Ser. A, vol. 185, No. 1001, Feb. 12, 1946, pp. 144-175.
11. W. M. Elsasser, "Heat Transfer by Infrared Radiation in the Atmosphere," *Harvard Meteorological Studies* No. 6, 1942, 107 pp.
12. R. Emden, "Über Strahlungsgleichgewicht und Atmosphärische Strahlung: Ein Beitrag zur Theorie der Oberen Inversion," *Sitzungsberichte*, Akademie der Wissenschaften, München, No. 1, 1913, pp. 55-142.
13. H. Flohn, "Kontinentalität und Ozeanität in der Freien Atmosphäre," *Meteorologische Zeitschrift*, vol. 60, 1943, pp. 325-331.
14. F. E. Fowle, "The Spectroscopic Determination of Aqueous Vapor," *Astrophysical Journal*, vol. 35, 1912, pp. 149-162.
15. F. E. Fowle, "The Transparency of Aqueous Vapor," *Astrophysical Journal*, vol. 42, 1915, pp. 394-411.
16. F. E. Fowle, "Water Vapor Transparency to Low Temperature Radiation," *Smithsonian Miscellaneous Collections*, vol. 68, No. 8, 1917.
17. D. M. Gates, D. G. Murcray, C. C. Shaw, and R. J. Herbold, "Near Infrared Solar Radiation Measurements by Balloon to an Altitude of 100,000 Feet," *Journal of the Optical Society of America*, vol. 48, 1959, pp. 1010-1016.
18. Geophysical Research Directorate, U. S. Air Force, *Handbook of Geophysics*, Rev. Ed., Macmillan and Co., New York, 1960.
19. E. Gold, "The Isothermal Layer of the Atmosphere and Atmospheric Radiation," *Proceedings of the Royal Society of London*, Ser. A, vol. 82, No. 551, Feb. 16, 1909, pp. 43-70.
20. R. M. Goody, "The Thermal Equilibrium at the Tropopause and the Temperature of the Lower Stratosphere," *Proceedings of the Royal Society of London*, Ser. A, vol. 197, 1949, pp. 487-505.
21. F. W. P. Götz, "Ozone in the Atmosphere," *Compendium of Meteorology*, American Meteorological Society, Boston, 1951, pp. 275-291.
22. E. H. Gowan, "The Effect of Ozone on the Temperature of the Upper Atmosphere," *Proceedings of the Royal Society of London*, Ser. A, vol. 120, 1928, pp. 655-669.
23. E. H. Gowan, "Ozonosphere Temperatures Under Radiative Equilibrium," *Proceedings of the Royal Society of London*, Ser. A, vol. 190, No. 1021, July 1947, pp. 219-226.
24. W. J. Humphreys, "Vertical Temperature-Gradients of the Atmosphere, Especially in the Region of the Upper Inversion—A Suggested Explanation of the Isothermal Layer," *Astrophysical Journal*, vol. 29, No. 1, Jan. 1909, pp. 14-32.
25. H. G. Houghton, "On the Annual Heat Balance of Northern Hemisphere," *Journal of Meteorology*, vol. 11, No. 1, Feb. 1954, pp. 1-9.
26. J. T. Houghton and J. S. Seeley, "Spectroscopic Observations of the Water Vapour Content of the Stratosphere," *Quarterly Journal of the Royal Meteorological Society*, vol. 86, No. 369, July 1960, pp. 358-370.
27. J. N. Howard, D. L. Burch, and D. Williams, "Near-Infrared Transmission Through Synthetic Atmospheres," *Geophysical Research Papers*, No. 40, Air Force Cambridge Research Center, AFCRC-TR-55-213, 1955, 244 pp.
28. E. C. Y. Inn and Y. Tanaka, "Absorption Coefficient of Ozone in the Ultraviolet and Visible Regions," *Journal of the Optical Society of America*, vol. 43, No. 10, Oct. 1953, pp. 870-873.
29. E. C. Y. Inn and Y. Tanaka, "Comparison of Recently Recorded Ozone Absorption Coefficients in the Visible and Ultraviolet Regions," *Conference on Ozone*, Armour Research Foundation, 1956, pp. 263-268.
30. F. S. Johnson, "The Solar Constant," *Journal of Meteorology*, vol. 11, No. 6, Dec. 1954, pp. 431-439.
31. L. D. Kaplan, "The Infrared Spectrum of Lower Stratosphere and Its Importance in the Heat Balance," *Scientific Proceedings of the International Union of Geodesy and Geophysics, Association of Meteorology, 10th General Assembly, Rome, Sept. 1954*, London, 1956, pp. 583-592.
32. H. H. Kimball, "Measurements of Solar Radiation Intensity and Determinations of Its Depletion by the Atmosphere," *Monthly Weather Review*, vol. 58, No. 2, Feb. 1930, pp. 43-52.
33. J. I. King, "Line Absorption and Radiative Equilibrium," *Journal of Meteorology*, vol. 9, No. 5, Oct. 1952, pp. 311-321.
34. A. Kochanski, "Cross Sections of the Mean Zonal Flow and Temperature Along 80° W.," *Journal of Meteorology*, vol. 12, No. 2, Apr. 1955, pp. 95-106.
35. J. London, G. Ohring, and I. Ruff, "Radiative Properties of the Stratosphere," *Final Report*, Contract AF19(604)-1285, Research Div. College of Engineering, New York University, 1956, 48 pp.
36. J. London, "A Study of the Atmospheric Heat Balance," *Final Report*, Contract AF19(122)-165, Research Div. College of Engineering, New York University, 1957, 99 pp.
37. J. McDonald, "Direct Absorption of Solar Radiation by Atmospheric Water Vapor," *Journal of Meteorology*, vol. 17, No. 3, June 1960, pp. 317-328.
38. L. Machta, "Meteorology and Radioactive Fallout," World Meteorological Organization, *Bulletin*, vol. 9, No. 2, Apr. 1960, pp. 64-70.
39. F. Möller, "Die Wärmestrahlung des Wasserdampfes in der Atmosphäre," *Beiträge zur Geophysik*, vol. 58, No. 1/2, 1941, pp. 11-61.
40. F. Möller, "Zur Erklärung der Stratosphärentemperatur," *Naturwissenschaften*, vol. 31, 1943, p. 148.
41. F. Möller and S. Manabe, "Über das Strahlungsgleichgewicht in der Atmosphäre," *Zeitschrift für Meteorologie*, (in press).
42. R. Mügge and F. Möller, "Zur Berechnung von Strahlungsströmen und Temperaturänderungen in Atmosphären von Beliebigen Aufbau," *Zeitschrift für Geophysik*, vol. 8, 1932, pp. 53-64.
43. R. J. Murgatroyd, P. Goldsmith, and W. E. H. Hollings, "Some Recent Measurements of Humidity from Aircraft Up to Heights of about 50,000 Ft. over Southern England," *Quarterly Journal of the Royal Meteorological Society*, vol. 81, No. 350, Oct. 1955, pp. 533-537.
44. R. J. Murgatroyd, "Some Recent Measurements by Aircraft of Humidity up to 50,000 Ft. in the Tropics and Their Relationship to the Meridional Circulation," *Proceedings of the Symposium on Atmospheric Ozone. Oxford, 20-25 July 1959*, I.U.G.G. Monograph No. 3, Paris, 1960, p. 30.
45. C. Normand, "Atmospheric Ozone and the Upper-Air Conditions," *Quarterly Journal of the Royal Meteorological Society*, vol. 79, No. 339, Jan. 1953, pp. 39-50.
46. Ny Tsi-Ze et Choong Shin-Piaw, "L'Absorption de la Lumière par l'Ozone entre 3050 et 3400 Å (Région des bandes de Huggins)," *Comptes Rendus, Académie des Sciences, Paris*, vol. 195, 1932, pp. 309-311.
47. Ny Tsi-Ze et Choong Shin-Piaw, "L'Absorption de la Lumière par l'Ozone entre 3050 et 2150 Å," *Comptes Rendus, Académie des Sciences, Paris*, vol. 196, 1933, pp. 916-918.
48. G. Ohring, "The Radiation Budget of the Stratosphere," *Scientific Report No. 1*, Contract AF19(604)-1738, Dept. of Meteorology and Oceanography, New York University, June 1957, 42 pp.

49. N. A. Phillips, "The General Circulation of the Atmosphere: A Numerical Experiment," *Quarterly Journal of the Royal Meteorological Society*, vol. 82, No. 352, Apr. 1956, pp. 123-164.
50. G. N. Plass, "The Influence of the 9.6 μ Ozone Band on the Atmospheric Infra-Red Cooling Rate," *Quarterly Journal of the Royal Meteorological Society*, vol. 82, No. 351, Jan. 1956, pp. 30-44.
51. G. N. Plass, "The Influence of the 15 μ Carbon Dioxide Band on the Atmospheric Infra-Red Cooling Rate," *Quarterly Journal of the Royal Meteorological Society*, vol. 82, No. 353, July 1956, pp. 310-324.
52. J. Pressman, "The Latitudinal and Seasonal Variations of the Absorption of Solar Radiation by Ozone," *Journal of Geophysical Research*, vol. 59, No. 4, Dec. 1954, pp. 485-498.
53. R. D. Richtmyer, *Difference Method for Initial Value Problems*, Interscience Publishers, Ltd., New York, 1957, (see p. 93).
54. O. E. T. Robert, "On Radiative Diffusion in the Atmosphere," *Proceedings of the Royal Society of Edinburgh*, vol. 50, 1929-30, pp. 225-242.
55. T. Sasumori, "The Temperature Effect on the Absorption of 15 microns Carbon Dioxide Band," *Science Reports of the Tohoku University, Ser. 5, Geophysics*, vol. 11, No. 3, Dec. 1959, pp. 149-161.
56. G. Simpson, "Some Studies in Terrestrial Radiation," *Memoirs of the Royal Meteorological Society*, vol. 2, No. 16, 1928, pp. 69-95.
57. J. Smagorinsky, General Circulation Experiments with the Primitive Equations: The Basic Experiment, 1961 (in preparation).
58. V. P. Starr and R. M. White, "Balance Requirements of the General Circulation," *Geophysical Research Papers* No. 35, Geophysical Research Directorate, Air Force Cambridge Research Center, 1954.
59. C. Størmer, "Height of Mother of Pearl Clouds Observed in Southern Norway During 1926-1934," *Nature*, vol. 145, 1940, pp. 221-222.
60. M. Summerfield, "Pressure Dependence of the Absorption in the 9.6 micron Band of Ozone," Doctoral Thesis, California Institute of Technology, 1941.
61. K. Telegadas and J. London, "A Physical Model of the Northern Hemisphere Troposphere for Winter and Summer," *Scientific Report No. 1*, Contract AF19(122)-165, Research Div., College of Engineering, New York University, Feb. 1954, 55 pp.
62. E. Tønnesberg and E. L. Olsen, "Investigations on Atmospheric Ozone at Nordlysobservatoriet, Tromsø," *Geofysiske Publikasjoner*, vol. 13, No. 12, 1943.
63. G. B. Tucker, "An Analysis of Humidity Measurements in the Upper Troposphere and Lower Stratosphere Over Southern England," *M.R.P. 1052*, S.C. III/235, Meteorological Research Committee, Air Ministry, England, 1957.
64. E. Vigroux, "Contributions a l'Etude Experimentale de l'Absorption de l'Ozone," *Annales de Physique*, vol. 8, 1953, pp. 709-762.
65. C. D. Walshaw, "Integrated Absorption by 9.6 μ Band of Ozone," *Quarterly Journal of the Royal Meteorological Society*, vol. 83, No. 357, July 1957, pp. 315-321.
66. L. R. Weber and H. M. Randall, "The Absorption Spectrum of Water Vapor Beyond 10 μ ," *Physical Review*, vol. 40, 1932, pp. 835-847.
67. G. Yamamoto and G. Onishi, "Absorption Coefficient of Water Vapour in the Far Infrared Region," *Science Reports of the Tohoku University, Ser. 5, Geophysics*, vol. 1, No. 2, Nov. 1949, pp. 71-75.
68. G. Yamamoto, "On a Radiation Chart," *Science Reports of the Tohoku University, Ser. 5, Geophysics*, vol. 4, No. 1, June 1952, pp. 9-23.
69. G. Yamamoto and G. Onishi, "Absorption of Solar Radiation by Water Vapor in the Atmosphere," *Journal of Meteorology*, vol. 9, No. 6, Dec. 1952, pp. 415-421.
70. G. Yamamoto, "Radiative Equilibrium of Earth's Atmosphere. I. The Grey Case," *Scientific Reports of the Tohoku University, Ser. 5, Geophysics*, vol. 5, No. 2, Oct. 1953, pp. 45-57.
71. G. Yamamoto, "Radiative Equilibrium of the Earth's Atmosphere. II. The Use of Rosseland's and Chandrasekhar's Means in the Line Absorbing Case," *Scientific Reports of the Tohoku University, Ser. 5, Geophysics*, vol. 6, No. 3, June 1955, pp. 127-136.